



Al-Mg and U-Pb chronological records of Erg Chech 002 ungrouped achondrite meteorite

Philip M Reger, Yvonne Roebbert, Wladimir Neumann, Abdelmouhcine Gannoun, Marcel Regelous, Winfried H Schwarz, Thomas Ludwig, Mario Tieloff, Stefan Weyer, Audrey Bouvier

► To cite this version:

Philip M Reger, Yvonne Roebbert, Wladimir Neumann, Abdelmouhcine Gannoun, Marcel Regelous, et al.. Al-Mg and U-Pb chronological records of Erg Chech 002 ungrouped achondrite meteorite. *Geochimica et Cosmochimica Acta*, In press, 343, pp.33-48. 10.1016/j.gca.2022.12.025 . hal-03924686

HAL Id: hal-03924686

<https://uca.hal.science/hal-03924686>

Submitted on 5 Jan 2023

HAL is a multi-disciplinary open access archive for the deposit and dissemination of scientific research documents, whether they are published or not. The documents may come from teaching and research institutions in France or abroad, or from public or private research centers.

L'archive ouverte pluridisciplinaire **HAL**, est destinée au dépôt et à la diffusion de documents scientifiques de niveau recherche, publiés ou non, émanant des établissements d'enseignement et de recherche français ou étrangers, des laboratoires publics ou privés.

Geochimica et Cosmochimica Acta

Al-Mg and U-Pb chronological records of Erg Chech 002 ungrouped achondrite meteorite --Manuscript Draft--

Manuscript Number:	GCA-D-22-00335R3
Article Type:	Article
Keywords:	Early Solar System; Planetary differentiation; achondrite; Al-Mg chronology; U-Pb chronology
Corresponding Author:	Philip M Reger CANADA
First Author:	Philip M. Reger
Order of Authors:	Philip M. Reger Yvonne Roebbert Wladimir Neumann Abdelmouhcine Gannoun Marcel Regelous Winfried H. Schwarz Thomas Ludwig Mario Trieloff Stefan Weyer Audrey Bouvier
Abstract:	<p>Achondrite meteorites are remnants of the earliest planetary differentiation processes in the Solar System. They have been used to anchor short-lived radiochronometers to absolute ages determined from long-lived radiochronometers. More specifically, when comparing the isotopic systematics of the short-lived ^{26}Al-^{26}Mg chronometer anchored to absolute U-corrected Pb-Pb ages, inferences about the distribution of ^{26}Al (half-life of $\sim 717\,000$ yr) in the protoplanetary disk can be evaluated. The ungrouped achondrite Erg Chech (EC) 002 has a distinct mineralogy and more evolved elemental composition compared to basaltic achondrites. In situ and solution ^{26}Al-^{26}Mg chronometry and ^{53}Mn-^{53}Cr chronometry suggest that EC 002 formed within ~ 0.7 to 2.2 Ma after the formation of Ca-Al-rich inclusions (CAIs), making it the oldest known sample of igneous crust in the Solar System (Barrat et al., 2021; Anand et al., 2022; Zhu et al., 2022; Fang et al., 2022). Here we present the U-corrected Pb-Pb age and ^{26}Al-^{26}Mg age obtained by MC-ICPMS solution analysis of the same mineral separate samples of EC 002. In addition, six merrillite grains were analyzed by in-situ SIMS to determine their Pb-Pb individual ages.</p> <p>The U isotope composition of EC 002 exhibits internal heterogeneities between leached pyroxene ($^{238}\text{U}/^{235}\text{U} = 137.766 \pm 0.027$) and the bulk rock ($^{238}\text{U}/^{235}\text{U} = 137.8190 \pm 0.0074$). The Pb isotope composition of progressively leached pyroxenes are characterized by radiogenic $^{206}\text{Pb}/^{204}\text{Pb}$ ratios (ranging from 41 to 23487). Using the U isotope composition of the leached pyroxenes, the resulting age of the $^{207}\text{Pb}/^{206}\text{Pb}$-$^{204}\text{Pb}/^{206}\text{Pb}$ isochron is 4565.87 ± 0.30 Ma (2σ). The weighted mean of the Pb-Pb ages of seven SIMS analyses of merrillites are 4564.3 ± 5.2 Ma (2σ). These similar ages (within uncertainty) indicate rapid cooling and the absence of significant thermal events after ~ 4559 Ma on the parent body of EC 002. The ^{26}Al-^{26}Mg isochron through a bulk, pyroxene, fine-grained and four plagioclase fractions defines an initial $^{26}\text{Al}/^{27}\text{Al}$ ratio of $[8.89 \pm 0.79] \times 10^{-6}$ corresponding to a formation age of 1.83 ± 0.12 Ma after CAIs ($[5.23 \pm 0.13] \times 10^{-5}$; Jacobsen et al., 2008). The initial ^{26}Al abundance is consistent with previous MC-ICP-MS ^{26}Al-^{26}Mg reported systematics for EC 002 (Fang et al., 2022), but 0.46 ± 0.13 Myr older than the in situ SIMS ^{26}Al-^{26}Mg age previously reported by Barrat et al. (2021). When anchored to the</p>

absolute Pb-Pb age of CV3 CAIs (4567.30 ± 0.16 Ma; Connelly et al., 2012), the Al-Mg model age of EC 002 is 4565.47 ± 0.20 Ma, slightly younger than its U-corrected Pb-Pb age.

The concordance of the Pb-Pb and ^{26}Al - ^{26}Mg ages of ungrouped CC achondrites when anchored to EC 002 suggest that ^{26}Al was homogeneously distributed between the NC and CC reservoirs at the time of their parent body accretion. Furthermore, the presence of internal U isotope heterogeneities found between mineral and whole-rock samples of EC 002 supports the need of U isotope analysis of meteoritic samples dated using the Pb-Pb chronometer.

Al-Mg and U-Pb chronological records of Erg Chech 002 ungrouped achondrite meteorite

Philip M. Reger^{1,*}, Yvonne Roebbert², Wladimir Neumann³, Abdelmouhcine Gannoun⁴, Marcel
Regelous⁵, Winfried H. Schwarz³, Thomas Ludwig³, Mario Tieloff³, Stefan Weyer², Audrey
Bouvier^{6,1}

¹ Department of Earth Sciences, Institute of Earth and Space Exploration, University of Western
Ontario, N6A 5B7 London, Ontario, Canada

² Institut für Mineralogie, Leibniz-Universität Hannover, 30167 Hannover, Germany

³ Institut für Geowissenschaften, Klaus-Tschira-Labor für Kosmochemie, Universität Heidelberg,
69120 Heidelberg, Germany

⁴ Laboratoire Magmas et Volcans, Université Clermont-Auvergne, F-63000 Clermont-Ferrand,
France

⁵ GeoZentrum Nordbayern, Friedrich-Alexander-Universität Erlangen-Nürnberg, 91054 Erlangen,
Germany

⁶ Bayerisches Geoinstitut, Universität Bayreuth, 95447 Bayreuth, Germany

* Correspondence: Dr. Philip Reger, preger@uwo.ca

22

23

24 Submitted to *Geochimica et Cosmochimica Acta* on April 21st 2022

25 Revised version submitted on November 5th, 2022

26 Abstract: 482 words

27 Main text: 11858 words

28 Tables: 8

29 Figures: 10

30 Supplementary Information: 3 Tables and 2 Figures

31

Abstract

Achondrite meteorites are remnants of the earliest planetary differentiation processes in the Solar System. They have been used to anchor short-lived radiochronometers to absolute ages determined from long-lived radiochronometers. More specifically, when comparing the isotopic systematics of the short-lived ^{26}Al - ^{26}Mg chronometer anchored to absolute U-corrected Pb-Pb ages, inferences about the distribution of ^{26}Al (half-life of $\sim 717\,000$ yr) in the protoplanetary disk can be evaluated. The ungrouped achondrite Erg Chech (EC) 002 has a distinct mineralogy and more evolved elemental composition compared to basaltic achondrites. *In situ* and solution ^{26}Al - ^{26}Mg chronometry and ^{53}Mn - ^{53}Cr chronometry suggest that EC 002 formed within ~ 0.7 to 2.2 Ma after the formation of Ca-Al-rich inclusions (CAIs), making it the oldest known sample of igneous crust in the Solar System (Barrat et al., 2021; Anand et al., 2022; Zhu et al., 2022; Fang et al., 2022). Here we present the U-corrected Pb-Pb age and ^{26}Al - ^{26}Mg age obtained by MC-ICPMS solution analysis of the same mineral separate samples of EC 002. In addition, six merrillite grains were analyzed by in-situ SIMS to determine their Pb-Pb individual ages. The U isotope composition of EC 002 exhibits internal heterogeneities between leached pyroxene ($^{238}\text{U}/^{235}\text{U} = 137.766 \pm 0.027$) and the bulk rock ($^{238}\text{U}/^{235}\text{U} = 137.8190 \pm 0.0074$). The Pb isotope composition of progressively leached pyroxenes are characterized by radiogenic $^{206}\text{Pb}/^{204}\text{Pb}$ ratios (ranging from 41 to 23487). Using the U isotope composition of the leached pyroxenes, the resulting age of the $^{207}\text{Pb}/^{206}\text{Pb}$ - $^{204}\text{Pb}/^{206}\text{Pb}$ isochron is 4565.87 ± 0.30 Ma (2σ). The weighted mean of the Pb-Pb ages of seven SIMS analyses of merrillites are 4564.3 ± 5.2 Ma (2σ). These similar ages (within uncertainty) indicate rapid cooling and the absence of significant thermal events after ~ 4559 Ma on the parent body of EC 002. The ^{26}Al - ^{26}Mg isochron through a bulk rock, pyroxene, fine-grained and four plagioclase fractions defines an initial $^{26}\text{Al}/^{27}\text{Al}$ ratio of $[8.89 \pm$

0.79] $\times 10^{-6}$ corresponding to a formation age of 1.83 ± 0.12 Ma after CAIs ($[5.23 \pm 0.13] \times 10^{-5}$; Jacobsen et al., 2008). The initial ^{26}Al abundance is consistent with previous MC-ICP-MS ^{26}Al - ^{26}Mg reported systematics for EC 002 (Fang et al., 2022), but 0.46 ± 0.13 Myr older than the *in situ* SIMS ^{26}Al - ^{26}Mg age previously reported by Barrat et al. (2021). When anchored to the absolute Pb-Pb age of CV3 CAIs (4567.30 ± 0.16 Ma; Connelly et al., 2012), the Al-Mg model age of EC 002 is 4565.47 ± 0.20 Ma, slightly younger than its U-corrected Pb-Pb age.

The concordance of the Pb-Pb and ^{26}Al - ^{26}Mg ages of ungrouped CC achondrites when anchored to EC 002 suggest that ^{26}Al was homogeneously distributed between the NC and CC reservoirs at the time of their parent body accretion. Furthermore, the presence of internal U isotope heterogeneities found between mineral and whole-rock samples of EC 002 supports the need of U isotope analysis of meteoritic samples dated using the Pb-Pb chronometer.

Keywords

early Solar System, planetary differentiation, achondrite, Al-Mg chronology, U-Pb chronology

1. Introduction

The use of radiometric dating has been a cornerstone of unravelling the mysteries surrounding the formation and early evolution of the Solar System. Of the various chronometers, the absolute Pb-Pb chronometer and the short-lived, relative ^{26}Al - ^{26}Mg chronometer have been particularly useful in dating extra-terrestrial materials. The ^{26}Al - ^{26}Mg chronometer can resolve events that took place within $\sim 30,000$ years, while the U-corrected Pb-Pb chronometer has, among other milestones, established the age of the Solar System between ~ 4567 and 4568 Ma by dating Ca-Al-rich inclusions in CV3 chondrites (CAIs; Amelin et al., 2010; Bouvier and Wadhwa, 2010; Connelly et al., 2012; Sanborn et al., 2019). Despite the merits of both these chronometers, questions remain about their significance. For instance, meaningful applications of the ^{26}Al - ^{26}Mg chronometer rely on a homogeneous initial distribution of the parent nuclide ^{26}Al ($T_{1/2} = 0.717$ Ma, NuDat 3.0, National Nuclear Data Center) between samples and a chronological reference (e.g., CAIs, achondrites). To determine absolute and accurate U-corrected Pb-Pb ages using the dual long-lived decay chains of ^{235}U to ^{207}Pb and ^{238}U to ^{206}Pb , the $^{238}\text{U}/^{235}\text{U}$ ratio needs to be precisely known. It was assumed that the $^{238}\text{U}/^{235}\text{U}$ ratio was invariant at 137.88 among early Solar System materials, until significant variations of up to 3.5% in different objects were discovered (Stirling et al., 2005; Amelin et al., 2010; Brennecka et al., 2010). The assumption of a homogeneous distribution of ^{26}Al in the protoplanetary disk has repeatedly been challenged, without a consensus in the scientific community emerging. Studies involving CAIs, amoeboid olivine aggregates (AOAs), bulk meteorites (Larsen et al., 2011), chondrules (Bollard et al., 2019) and angrites (Schiller et al., 2015) suggested an initial $^{26}\text{Al}/^{27}\text{Al}$ ratio in the inner Solar System around 1×10^{-5} , about 80% lower than the canonical value of $\sim 5.2 \times 10^{-5}$ (Jacobsen et al., 2008). Other studies have disagreed with these conclusions (e.g., Wasserburg et al., 2012; Kita et al., 2013; Gregory et al., 2020). In

particular, combined U-corrected Pb-Pb and ^{26}Al - ^{26}Mg dating of achondrites, e.g., angrites or unique, ungrouped meteorites, have been frequently utilized to evaluate the distribution of ^{26}Al within the protoplanetary disk (e.g., Bouvier et al., 2011; Schiller et al., 2015; Wimpenny et al., 2019). The Pb-Pb and ^{26}Al - ^{26}Mg ages of some meteorites that formed in the non-carbonaceous inner Solar System (NC reservoir; Warren, 2011; Kruijer et al., 2020), such as the angrite D'Orbigny (Amelin, 2008b; Schiller et al., 2015; Tissot et al., 2017), used as an anchor meteorite for short-lived radionuclide chronometers, and the unique achondrite Asuka 881394 (Wadhwa et al., 2009; Hublet et al., 2017; Wimpenny et al., 2019) do not match in model ages when anchored to CAIs from the CV3 chondrites Efremovka and Allende using their reported U-corrected Pb-Pb ages (Connelly et al., 2012) and canonical $^{26}\text{Al}/^{27}\text{Al}$ ratio of $[5.23 \pm 0.13] \times 10^{-5}$ (Jacobsen et al., 2008). Conversely, the Pb-Pb and ^{26}Al - ^{26}Mg systematics of achondrites that formed in the carbonaceous chondrite (CC) reservoir of the outer Solar System, such as NWA 6704 (Amelin et al., 2019; Sanborn et al., 2019) and NWA 2976 (Bouvier et al., 2011b), exhibit concordant U-corrected Pb-Pb and ^{26}Al - ^{26}Mg ages when anchored to the absolute age of CAIs of 4567.30 ± 0.16 Ma (Connelly et al., 2012), suggesting a homogeneous distribution of ^{26}Al between CAIs and CC meteorites. The discordance between U-corrected Pb-Pb and ^{26}Al - ^{26}Mg ages of some NC meteorites has been interpreted by different studies to reflect either heterogeneity of ^{26}Al in the Solar System (Schiller et al., 2015), or that the ^{26}Al - ^{26}Mg systematics were disturbed through thermal metamorphism or shock heating from impact events (Sanborn et al., 2015; Koefoed et al., 2016; Sanborn et al., 2019; Wimpenny et al., 2019).

In order to further evaluate the distribution of ^{26}Al in the early Solar System, we have used both the Pb-Pb and ^{26}Al - ^{26}Mg chronometers to date the formation of the unique achondrite Erg Chech 002. Erg Chech 002 is a recent meteorite find with an unusual chemistry and mineralogy: (1) the

whole-rock composition is comparable to terrestrial andesites in silica and alkaline element concentrations (Barrat et al., 2021) and (2) it contains large (up to 9 cm) orthopyroxene megacrysts (Gattacceca et al., 2021) in a groundmass of sodic plagioclase, pigeonite and silica (Fig. 1). Geochemically, EC 002 exhibits a distinct trace element pattern compared to other andesitic meteorites, with no significant anomalies in alkali and high field-strength elements relative to CI chondrites (Barrat et al., 2021; Nicklas et al., 2022). Highly siderophile elements show fractionation between the compatible and incompatible elements that suggest metal-silicate separation occurred on the parent body of EC 002 (Nicklas et al., 2022).

Mass-independent $\Delta^{17}\text{O}$ values of EC 002 suggest an affinity with four anomalous eucrites, Bunburra Rockhole, EET 92023, Emmaville and Asuka 881394, but these meteorites are mineralogically different from EC 002 (Gattacceca et al., 2021). The O isotope composition, the negative Tm anomaly of the whole-rock (Barrat et al., 2021), as well as the Cr and Nd stable isotope anomalies (Anand et al., 2022; Fang et al., 2022; Zhu et al., 2022) indicate accretion of the EC 002 parent body in the NC reservoir. The elemental composition supports formation by partial melting of a chondritic precursor, followed by rapid cooling after cooling to 900°C, likely by excavation or ejection from an impact event (Barrat et al., 2021).

EC 002 was first dated by in situ ^{26}Al - ^{26}Mg analysis using secondary ionization mass spectrometry (SIMS), as well as noble gas geochemistry (Barrat et al., 2021). The Al-Mg systematics result in an initial $^{26}\text{Al}/^{27}\text{Al}$ ratio of $[5.72 \pm 0.07] \times 10^{-6}$ and an age of 2.29 ± 0.04 Ma after CAI formation, making it the oldest igneous meteorite found to date. A subsequent study of the ^{26}Al - ^{26}Mg chronology by MC-ICP-MS reported a different initial $^{26}\text{Al}/^{27}\text{Al}$ ratio of $[8.89 \pm 0.09] \times 10^{-6}$, resulting in an age of 1.83 ± 0.04 Ma after CAI formation (Fang et al., 2022). Additionally, the formation age of EC 002 was modelled at 4565.6 ± 0.6 Ma and 4566.6 ± 0.6 Ma by two separate

studies using the short-lived ^{53}Mn - ^{53}Cr chronometer, albeit anchored to the D'Orbigny angrite (Anand et al., 2022; Zhu et al., 2022). To get a better constraint on the crystallisation history of EC 002, assess its potential as a new anchor for short-lived radionuclides and to further evaluate the distribution of ^{26}Al in the early Solar System, we analyzed the Mg, Pb and U isotope compositions of whole-rock and mineral fractions from the same sample piece by multi collector inductively coupled plasma mass spectrometry (MC-ICP-MS) to determine the ^{26}Al - ^{26}Mg and U-corrected Pb-Pb ages. We also analysed merrillite Ca-phosphates by *in-situ* secondary ion mass spectrometry (SIMS) Pb-Pb analysis to constrain the crystallization history and thermal records of EC002.

2. Methods

2.1 Sample preparation

For U-Pb and Al-Mg studies, a ~ 600 mg section of Erg Chech 002 (from Ben Hoefnagels, Big Bang Meteorites) was rinsed in acetone and water, prior to being crushed in an agate mortar. Roughly 120 mg were taken as a bulk rock fraction. Pyroxene and feldspar minerals were separated by hand-picking under binoculars, with repeated crushing and sieving. Eight feldspar fractions were hand-picked, along with a pyroxene and a fine-grained (<60 μm) fraction for Mg isotope analysis.

2.2 Characterisation and SIMS Pb-Pb dating of phosphates

A 1-inch polished section mounted in epoxy was prepared from a 0.75g slice of EC 002 (Mirko Graul Meteorite) at the Bayerisches Geoinstitut (BGI). The section was first carbon-coated and analysed to obtain multi-field BSE-EDS element maps (Fig. 1; preselected to be Na, Mg, Al, Si,

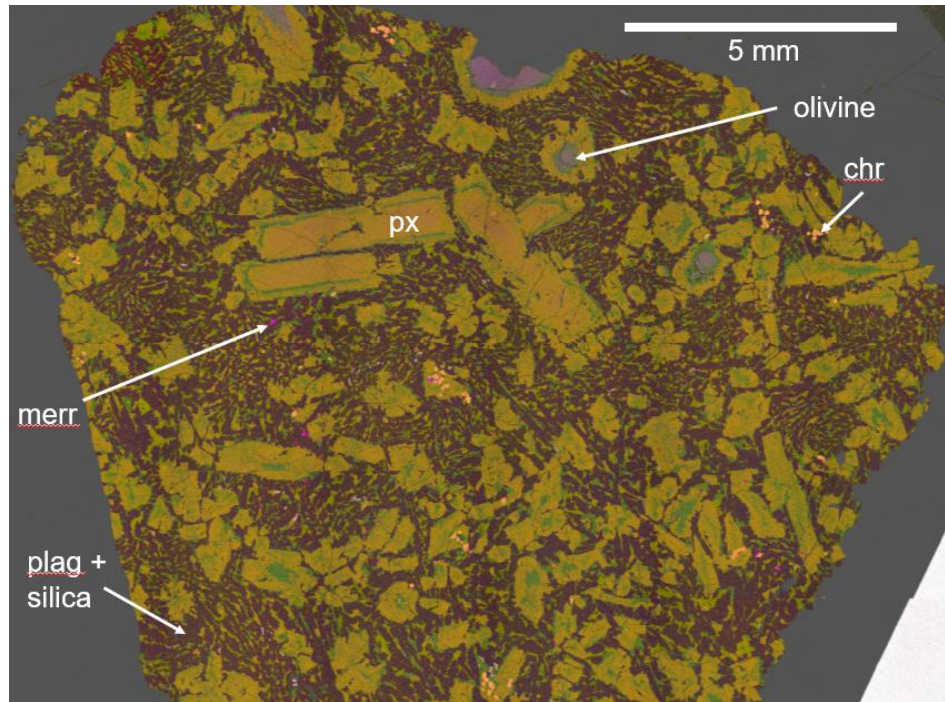
162 P, O, Fe, Ca, Ti, Zr, Cr, Ni, S, Cl) using a focused ion beam scanning electron microscopy (FEI
 163 Scios FIB-SEM) at BGI. For this purpose, the electron beam was tuned to 20 kV and 1.6 nA. We
 164 selected six merrillite grains for SIMS analyses.

165 Further petrographic observations were carried out at BGI using a Zeiss Gemini 1530 scanning
 166 electron microscope operated at 20 kV under BSE-EDS mode. Mineral compositions were
 167 measured using a JEOL JXA 8200 electron microprobe equipped with five spectrometers operated
 168 at 15 kV and 15 nA with $\sim 1\ \mu\text{m}$ focused electron beam ($5\ \mu\text{m}$ for merrillites) and counting time of
 169 20s on peak and 10s on background (10s on peak for Na, Cl and F, and 5s on background to reduce
 170 the beam induced damage and loss of volatile during analysis). The standards used were: Na and
 171 Si (albite), Ca (wollastonite or apatite), K (orthoclase), Mg (enstatite), Fe (Fe metal), Mn and Ti
 172 (MnTiO_3), Al (spinel), Ni (Ni metal), Cr (Cr metal), and P (apatite).

173 For SIMS, the carbon coating of the same polished mount of EC 002 was removed. The mount
 174 was cleaned with alcohol, dried, and coated with a 50 nm gold film before SIMS analysis. High
 175 precision ^{207}Pb - ^{206}Pb phosphate dating was performed using a Cameca IMS 1280-HR type
 176 secondary ion mass spectrometer (SIMS) at the Heidelberg Ion Probe (HIP), Universität
 177 Heidelberg. Duoplasmatron ion source was operated to generate a primary O^+ ion beam with 23
 178 kV impact energy, 20-40 nA current and beam size of 20-30 μm on sample surface. During each
 179 analysis, a two-minute pre-sputtering was applied to remove potential surface contamination.

180 Positive secondary ions of $^{40}\text{Ca}_2^{31}\text{P}^{16}\text{O}_4^+$, $^{204}\text{Pb}^+$, $^{206}\text{Pb}^+$, $^{207}\text{Pb}^+$, $^{238}\text{U}^+$, $^{238}\text{U}^{16}\text{O}^+$ were extracted,
 181 mass filtered at a mass resolution ($M/\Delta M$) of ~ 4000 before detected sequentially in a low-noise
 182 ion-counting electron multipliers for 1s, 20s, 10s, 10s, 10s and 6s, respectively under single
 183 collection mode. Thirty cycles per analysis were typically applied for better statistics.

184 $^{40}\text{Ca}_2^{31}\text{P}^{16}\text{O}_4^+$ was used for peak centering and $^{238}\text{U}^{16}\text{O}^+$ for calculating U and Pb secondary ion
185 yields.



186
187 **Figure 1:** Backscattered electron image overlaid with energy dispersive spectroscopy composed
188 as a multi-field phase colored map of Erg Chech 002 (Si in yellow, Na in dark blue, Al in grey,
189 Mg in red, Ca in pink) polished mount used for the SIMS analyses. Large pyroxene megacrysts
190 and rounded olivine crystals are surrounded by groundmass of sodic plagioclase, pigeonite and
191 accessory chromite, merrillite and silica polymorphs.

192

193

194 2.3 Determination of $^{27}\text{Al}/^{24}\text{Mg}$ ratios

195 A bulk rock fraction consisting of roughly 120 mg, one pyroxene and eight feldspar mineral
196 fractions prepared for Mg isotope analysis were dissolved in a 29 M HF- 15 M HNO_3 (5:1) mixture
197 at 120 °C, before being dried down and re-dissolved in 15M HNO_3 . The samples were dried down

again and then converted to its chloride form with 6 M HCl. Determination of the $^{27}\text{Al}/^{24}\text{Mg}$ ratios of the mineral separates was performed using a Thermo Fischer iCAP Qc quadrupole ICP-MS at the University of Western Ontario (UWO). Of the eight feldspar fractions, after an initial analysis, those with similar $^{27}\text{Al}/^{24}\text{Mg}$ ratios were combined in order to maximize Mg content, allowing for analysis at higher concentrations, without sacrificing the spread of $^{27}\text{Al}/^{24}\text{Mg}$ ratios. This resulted in four feldspar fractions, alongside the bulk rock, pyroxene and fine-grained fractions. During analysis, gravimetrically prepared Al-Mg solutions, ranging from $^{27}\text{Al}/^{24}\text{Mg}$ ratios of 0.001 to 50, were used to calibrate $^{27}\text{Al}/^{24}\text{Mg}$ ratios of the samples. Terrestrial standards BCR-2 and San Carlos olivine, and bulk rock CV3 chondrite Allende were analyzed with the samples to verify the accuracy of the analysis and are reported alongside their isotopic compositions in Table 1. Uncertainties associated with $^{27}\text{Al}/^{24}\text{Mg}$ ratios is $\pm 5\%$, with exception of the bulk rock fraction, which in two separate analyses resulted in distinct $^{27}\text{Al}/^{24}\text{Mg}$ ratios. To account for the increased uncertainty, the error there is the 2SE of the average of both analyses.

2.4 Magnesium isotope analysis

An aliquot equivalent to 0.6 mg of the bulk rock fraction and corresponding to $\approx 20\ \mu\text{g}$ Mg was set aside for Mg separation, along with the pyroxene, fine-grained and feldspar fractions. We used a two-stage ion-exchange chromatography protocol, following a modified version of the protocol described by Wombacher et al. (2009).

The protocol uses about 1.2 ml of AG50W-X8 (200-400 mesh) resin deposited within HCl-cleaned BioRad® plastic columns. For the first stage, the columns and resin are cleaned again together with ca. 20 ml of 6 M HCl. The resin is then conditioned with 3.6 ml of 10 M HCl. The sample is taken up in 0.3 ml 10 M HCl and then loaded onto the columns, before Mg and other matrix

elements (such as Al, Cr and Ni) are eluted by 3.2 ml of 10 M HCl. Subsequent Ca and Fe elution are accomplished by adding 15 ml of 8 M HCl and 20 ml of 4 M HCl, respectively, to the columns. To ensure sufficient recovery of Mg, the first 0.8 ml of the Ca elution step are collected separately and dried down. The same procedure is repeated a second time with the separate cut which is then collected and combined with the 3.2 ml from the previous run. Magnesium is then further separated from the remaining matrix elements by a third stage, using the same columns and resin as the previous stages. The resin is first conditioned with 3.6 ml 0.4 M HCl before the sample is loaded onto the column in 0.3 ml of 0.4 M HCl. Remaining matrix elements are eluted by adding 33.6 ml of 0.4 M HCl and then 7.2 ml of 0.15 M HF. For Mg elution, 1 ml of 1 M HCl is added before an additional 20 ml are added (Table 2). This method results in a total yield of > 99.6 % of Mg. We used dissolved homogenized powders of the San Carlos olivine and the Allende CV3 meteorite as inter-laboratory secondary standards, that underwent the full protocol with each set of columns. To evaluate that the column chemistry did not introduce any fractionation on Mg isotopes, a pure Mg standard solution was analyzed without column processing, with column processing, and after the solution being added to the Mg-free matrices of terrestrial standards BCR-2 and BIR-1. Between these analyses, no resolvable differences in Mg isotope compositions were found (Table 1).

Magnesium isotope compositions of EC 002 fractions were analyzed by a Thermo Fisher Neptune Plus MC-ICP-MS at the Friedrich-Alexander-Universität (FAU) in Erlangen. The ^{24}Mg , ^{25}Mg and ^{26}Mg ion beams were measured simultaneously on the L4, Center and H4 Faraday cups, respectively, with a 10^{10} amplifier on the L4 cup, and run in medium resolution mode with a Jet sample cone and H skimmer cone interface. The sample and standard solutions were diluted to approximately 300 ppb (≈ 90 V on ^{24}Mg), where Mg amounts allowed, in 2% HNO_3 and matched

to within 5% or less of their concentrations. Solutions were introduced using a Cetac Aridus II desolvating nebulizer system. Standard-sample bracketing with the DSM-3 standard was used to correct for mass fractionation and instrumental drift. Generally, analyses consisted of four sample measurements bracketed by five standard measurements, with each measurement consisting of a peak center, 20 cycles at 8.4 s of integration time followed by 150 s of wash time. The instrumental background was measured prior to each sample and standard analysis. Total procedural blanks were less than 5 ng, a negligible amount relative to the amount of Mg in the samples ($\approx 75 \mu\text{g}$). We report our Mg isotope data in δ -notation (in per mil), the relative differences of $^x\text{Mg}/^{24}\text{Mg}$ ratios of the sample to the bracketing standard, where $x = 25$ or 26 :

$$\delta^x\text{Mg} = ([^x\text{Mg}/^{24}\text{Mg}]_{\text{sample}} / [^x\text{Mg}/^{24}\text{Mg}]_{\text{standard}} - 1) \times 1000 \quad (\text{Eq. 1})$$

Mass-independent variations in ^{26}Mg due to ^{26}Al decay ($\delta^{26}\text{Mg}^*$) were determined by internally normalizing the measured $^{26}\text{Mg}/^{24}\text{Mg}$ ratio to $^{25}\text{Mg}/^{24}\text{Mg} = 0.12663$ (Catanzaro et al., 1966) using the exponential law with fractionation factor $\beta = 0.511$:

$$\delta^{26}\text{Mg}^* = (\delta^{26}\text{Mg} - (1 + \delta^{25}\text{Mg}/1000)^{(1/\beta)} - 1) \times 1000 \quad (\text{Eq. 2})$$

Table 1: Al-Mg data for Mg solution standard Cambridge-1, terrestrial rock standard San Carlos olivine, and bulk rock CV3 chondrite Allende, as well as unprocessed and processed standard solution isotope compositions to verify the absence of fractionation effects during column chemistry. n.r.: not reported.

Standards	$^{27}\text{Al}/^{24}\text{Mg}$	\pm	$\delta^{25}\text{Mg}$ [‰]	2SE	$\delta^{26}\text{Mg}^*$ [‰]	2SE	n
Cambridge-1			-1.374	0.020	-0.005	0.006	22
<i>literature</i> ^a			-1.343	0.036	n.r.	n.r.	49
<i>literature</i> ^b			-1.335	0.032	n.r.	n.r.	
San Carlos olivine	0.0021	0.0009	-0.162	0.009	-0.005	0.005	9
<i>literature</i> ^c	0.0031	0.0004	-0.16	0.07	0.00	0.05	36

Allende	0.1300	0.0039	-0.174	0.026	0.013	0.009	4
<i>literature</i> ^c	0.1294	0.0007	-0.16	0.03	0.03	0.05	
BCR-2	3.796	0.052					
<i>literature</i> ^c	3.76	0.04					
UWO ICP Std ^d			-0.329	0.027	0.018	0.022	12
UWO ICP Std ^e			-0.296	0.027	-0.013	0.031	8
UWO ICP Std ^f			-0.323	0.020	0.006	0.041	8
UWO ICP Std ^g			-0.309	0.023	-0.003	0.033	16
UWO ICP Std ^h			-0.318	0.018	0.006	0.021	28

^a From An and Huang (2014). ^b From Vogl et al. (2020). ^c From Bouvier et al. (2013). ^d Unprocessed. ^e Column processed. ^f Added to Mg-free matrices of terrestrial standards BCR-2 and BIR-1, column processed. ^g All column-processed combined (b+c). ^h All standard solution measurements combined (a+b+c).

268 **Table 2:** Three-stage Mg separation scheme modified from Wombacher et al. (2009)

Stage 1 + 2			Stage 3		
Resin: 1.2 ml of AG50W-X8 (200-400 mesh)					
Step	Acid	Volume [ml]	Step	Acid	Volume [ml]
Resin cleaning	4 M HCl	ca. 20	Resin conditioning	0.4 M HCl	3.6
Resin conditioning	10 M HCl	3.6	Load sample	0.4 M HCl	0.3
Load sample	10 M HCl	0.3	Matrix elution	0.4 M HCl	33.6
Mg + matrix elution	10 M HCl	3.2	Be, Ti, Al elution	0.15 M HF	7.2
Post-Mg step	8 M HCl	0.8	Pre-Mg step	1 M HCl	1
Ca elution	8 M HCl	14.2	Mg elution	1 M HCl	20
Fe elution	4 M HCl	10	Wash out	6 M HCl	5
Wash out	4 M HCl	10			

269

270

271 2.5 Lead isotope analysis

272 Pervasive terrestrial Pb contamination (Pb_c) of meteoritic samples is a major concern. Meaningful

273 ^{207}Pb - ^{206}Pb isochrons are linear arrays of a two-component system made up of radiogenic Pb (Pb_r),

274 produced by the decay of ^{235}U and ^{238}U , and, in most cases, initial Pb (Pb_i). Adding a third

275 component, Pb_c , to this system can pull data points off the $Pb_r + Pb_i$ line towards the Pb_c isotope

composition, affecting the linearity of the isochron. This requires effective removal of all Pb_c from samples (e.g., Connelly et al., 2017). Alternatively, Pb-Pb ages can also be accurately calculated from linear arrays made of Pb_r and Pb_c , if the sample contains no initial Pb (Pb_i). This is achieved through a step-wise dissolution procedure where crushed samples were leached first by weak acids to remove surface contamination before increasingly strong acids were used to dissolve minerals (Connelly and Bizzarro, 2009). The pyroxene fraction, totalling ~ 61 mg, underwent such a procedure as described in Bouvier et al. (2011). The sample was ultrasonicated in 0.5 M HBr, then Milli-Q water and twice in 0.5 M HNO_3 for 15 minutes each. Subsequent steps involved a hot-plate fluxing in 6 M HCl and 7 M HNO_3 (twice) at 120°C for an hour, ultrasonication in 1 M HF for an hour and 12-hour-long hot-plate fluxing at 90°C in 1 M HF (Table 3). Since the first three steps are designed to remove terrestrial Pb and are unlikely to have any chronological meaning (e.g., Merle et al., 2020), these were collected all together in one beaker. Steps 5 and 6 (both 7 M HNO_3) were also mixed, as the amount of Pb (0.13 ng total) would have been insufficient for a precise determination of the Pb isotope ratios if these two leaching steps had been analyzed separately.

The collected washes from each step were then dried down before being dissolved in a conc. HF- HNO_3 mixture for ~48 hrs. After ultrasonication for an hour and subsequent drying down, the samples are re-fluxed in conc. HNO_3 , before being ultrasonicated once again and taken up in 6 M HCl to convert the samples to their chloride form. Prior to Pb separation, the fractions were analyzed for their U and Pb concentrations using Thermo Fischer iCAP Qc quadrupole ICP-MS at the University of Western Ontario (UWO).

Table 3: Leaching protocol for samples prepared for Pb isotopic analysis.

Step	Acid	Processing	Duration	Repeat	Collected as...	
1	0.5 M HBr	Ultrasonication washing	15 min	once	Wash-1 (W1)	Combined as W1-3
2	Water	Ultrasonication washing	15 min	once	Wash-2 (W2)	
3	0.5 M HNO ₃	Ultrasonication washing	15 min	twice	Wash-3 (W3)	
4	6 M HCl	Hot plate fluxing at 120°C	1 hr	once	Wash-4 (W4)	Combined as W5+6
5	7 M HNO ₃	Hot plate fluxing at 120°C	1 hr	once	Wash-5 (W5)	
6	7 M HNO ₃	Hot plate fluxing at 120°C	1 hr	once	Wash-6 (W6)	
7	1 M HF	Ultrasonication washing	1 hr	once	Wash-7 (W7)	
8	1 M HF	Hot plate fluxing at 90°C	12 hrs	once	Wash-8 (W8)	

299

300 For Pb separation, PTFE columns with 100 µl of AG1-X8 (200-400 mesh) anion-exchange resin
301 are used following the procedure described in Bouvier et al. (2007), which was based on Marsh et
302 al. (1978). Before loading, the samples are dried down and taken up in 1.5 M HBr and centrifuged
303 to separate any remaining undissolved materials. Matrix elements are first eluted using 1.5 M HBr
304 after the sample load. Lead is finally eluted using 0.5 M HNO₃. This procedure is repeated a second
305 time to guarantee sufficient purification of Pb from matrix elements. The eluted matrix elements
306 were collected together for U isotope analysis.

Lead isotope compositions were determined using a Thermo Fisher *Neptune Plus* MC-ICP-MS equipped with a Cetac Aridus II desolvating nebulizer at Université Clermont-Auvergne (UCA) and followed the protocols of Ancellin et al. (2019). The total Pb masses in the various leachates range from 0.13 ng to 3 ng and were taken up in 0.5 to 1.5 ml of 0.05M HNO₃, depending on their Pb concentration. Sample and standard solutions were both doped with the NBS 997 Tl standard to a concentration of 1 ppb and bracketed with the NBS 981 Pb standard (Abouchami et al., 2000) to correct internally and externally for instrumental mass fractionation. In addition, the radiogenic NBS 983 Pb standard was included in the analytical sessions as a secondary standard. Before every standard and sample measurement, a background measurement with baseline analysis was taken, which was subtracted from the standards or samples during data reduction. Peak center and baseline analysis were performed on all standard measurements but only on samples diluted in 1.5 ml of 0.05M HNO₃, to ensure sufficient material for was available for the isotopic analysis. Two samples, where enough ²⁰⁴Pb was present, were analyzed in a Faraday cup (FC) setup (EC W1-3 and ECW4). The other samples were analyzed with a secondary electron multiplier (SEM) on ²⁰⁴Pb, as the intensity in a FC setup would be below 0.3 mV. This setup has the disadvantage that ²⁰⁸Pb cannot be measured on H4 due to the fixed spacing imposed by the pin attaching H3 and H4 (Table 4). Sample analyses consisted of 60 cycles with 8.4 s integration time in the FC setup, whereas the analyses in the SEM setup consisted of only 25 cycles, with no peak center or baseline analysis.

The measured Pb isotopic data were reduced offline in Excel and R, and “inverse” isochrons were calculated using IsoplotR (Vermeesch, 2018) and Isoplot 4.15 in Excel (Ludwig, 2008). Total procedural blanks ranged from 0.3 to 1.8 pg, resulting in sample/blank ratios from 131 to 3808, and compositions were corrected accordingly, following the equations provided in the Appendix

of Bouvier et al. (2007). Errors on $^{204}\text{Pb}/^{206}\text{Pb}$ and $^{207}\text{Pb}/^{206}\text{Pb}$ ratios for isochron regression were either the correlated errors or the daily external reproducibility of the NBS 981 or NBS 983 standards (depending on which standard is more representative of the sample ratios), whichever is larger.

The full session Pb isotope data averages are reported in Table 5.

Table 4: Overview of cup configurations used for Pb isotope analysis with all Faraday cups (FC) or with central Secondary Electron Multiplier (SEM).

Cup	L3	L2	L1	C (or SEM)	H1	H2	H3
Pb (FC)	^{202}Hg	^{203}Tl	^{204}Pb	^{205}Tl	^{206}Pb	^{207}Pb	^{208}Pb
Pb (SEM)		^{202}Hg	^{203}Tl	^{204}Pb	^{205}Tl	^{206}Pb	^{207}Pb

2.6 Uranium isotope analysis

Analysis of the U isotope composition of a bulk rock sample and leached pyroxenes (included W5+6, W7, W8 and R) of EC 002 were performed with a Neptune MC-ICP-MS at the Leibniz Universität Hannover, following the protocols of Roebbert et al. (2021). The collected matrix elements of two aliquots of the terrestrial standard BCR-2, equal to ~ 5 ng and ~ 20 ng of U that underwent prior Pb separation (as for EC 002), were analyzed along with the meteorite samples to ensure that no U isotope fractionation occurred during the separation of Pb (Table 6). The ^{236}U - ^{233}U double-spike solution IRMM 3636 was used to correct for instrumental mass-bias (Richter et al., 2010). Each sample was analyzed twice, bracketed by the CRM-112a standard, over 60 cycles at 4 s integration time. Concentrations between standards and samples were individually matched and intensities on ^{238}U were 2.5 V and 12 V for the leached pyroxene and the bulk rock fraction,

respectively. Because of the relatively low ion beams, all U isotopes, including ^{238}U , were measured using amplifiers with 10^{-11} Ohm resistors. The standard IRMM 184 was analyzed along with the samples and its results are reported in Table 6.

3. Results

3.1 Al-Mg systematics

Magnesium isotope compositions and $^{27}\text{Al}/^{24}\text{Mg}$ ratios of the analyzed mineral fractions of EC 002 are summarized in Table 7. The $^{27}\text{Al}/^{24}\text{Mg}$ ratios span a range from 0.98 for the Px fraction to 34.4 in feldspars. Excesses in ^{26}Mg are not resolved from the terrestrial fractionation line for the bulk rock and Px fractions at $\delta^{26}\text{Mg}^* = 0.013 \pm 0.020\text{‰}$ and $0.010 \pm 0.010\text{‰}$, respectively. In the feldspar fractions and fines fraction, radiogenic ^{26}Mg excesses are resolved and range from $0.132 \pm 0.010\text{‰}$ to $2.058 \pm 0.015 \text{‰}$. A regression line through the data is obtained with Isoplot 4.15 (Ludwig, 2008), with a slope corresponding to the $^{26}\text{Al}/^{27}\text{Al}$ at the time of crystallization of $[8.89 \pm 0.79] \times 10^{-6}$ and an y-intercept $\delta^{26}\text{Mg}^*_0$ of $-0.058 \pm 0.026\text{‰}$ (both 2σ), representing the initial Mg isotope composition at time of crystallization (MSWD = 4.6). This $^{26}\text{Al}/^{27}\text{Al}_0$ corresponds to a crystallization age of 1.83 ± 0.12 Ma after CAI formation (Fig. 2a). This corresponds to an absolute age of 4565.47 ± 0.20 Ma when anchored to the canonical $^{26}\text{Al}/^{27}\text{Al}$ value of $[5.23 \pm 0.13] \times 10^{-5}$ (Jacobsen et al., 2008) and the absolute age of CAIs at 4567.30 ± 0.16 Ma (Connelly et al., 2012). When anchored to the D'Orbigny angrite (Pb-Pb age: 4563.51 ± 0.29 (Amelin, 2008b; Tissot et al., 2017), initial $^{26}\text{Al}/^{27}\text{Al}$: $[3.98 \pm 0.15] \times 10^{-7}$ (Schiller et al, 2015), $[5.06 \pm 0.15] \times 10^{-7}$ (Spivak-Birndorf et al., 2009)), the ^{26}Al - ^{26}Mg formation age of EC 002 is 4566.72 ± 0.32 Ma and 4566.47 ± 0.40 Ma, calculated from the initial $^{26}\text{Al}/^{27}\text{Al}$ ratios of Schiller et al. (2015) and Spivak-

Birndorf et al. (2009), respectively. These ages are 1.26 ± 0.38 Myr and 1.01 ± 0.45 Myr, respectively, older than when anchored to CAIs.

Regressing the subset of feldspar fractions results in an initial $^{26}\text{Al}/^{27}\text{Al}$ of $[8.36 \pm 0.49] \times 10^{-6}$ and a $\delta^{26}\text{Mg}^*_0$ of $-0.010 \pm 0.032\text{‰}$ (MSWD = 0.0017), equal within the stated uncertainties of the regression through the complete dataset (Fig. 2b).

The $\delta^{25}\text{Mg}$ values of EC 002 fractions lie between $-0.729 \pm 0.012\text{‰}$ and $-1.104 \pm 0.013\text{‰}$, which are distinctly lighter than the compositions of the terrestrial San Carlos olivine and the CV3 chondrite Allende.

3.2 Uranium isotope composition

The results for the $^{238}\text{U}/^{235}\text{U}$ ratios in both the bulk rock and the re-combined W5-R leachates and residue of EC 002 are summarized in Table 6. Both samples were measured twice, with their weighted average $^{238}\text{U}/^{235}\text{U}$ ratios being 137.819 ± 0.010 for the bulk rock, and 137.766 ± 0.027 for the leachates (both 2σ). The uncertainty associated with the analyses, particularly on the leachates, is mainly due to the low U concentration of this sample (2.5 V on ^{238}U from ≈ 5 ng U).

389 **Table 5:** Mass, Pb and U elemental data, and Pb isotope data for EC 002 and full session Pb isotope data for standards NBS 981 and
390 NBS 983. Nantan model ages are calculated from the primordial Pb isotope composition, represented by the Nantan troilite (Blichert-
391 Toft et al., 2010). SK model ages are calculated from the modern terrestrial Pb composition as given by Stacey and Kramers (1975).

Sample	mass [mg]	Pb [ng]	U [ng]	Sample/ Blank	$^{206}\text{Pb}/^{204}\text{Pb}$ raw	$^{204}\text{Pb}/^{206}\text{Pb}$	2SE [%]	$^{207}\text{Pb}/^{206}\text{Pb}$	2SE [%]	Nantan model age [Ma]	±	SK model age [Ma]	±
EC-W1-3 *	1.6	3.2	2.2	3808	41.5	0.024092	0.015	0.72121	0.0024	4529.73	0.10	4571.38	1.54
EC-W4 *	1.0	1.3	6.5	1549	42.5	0.023515	0.035	0.71755	0.0054	4526.72	0.16	4565.57	1.49
EC-W5+6 *	0.3	0.1	0.2	131	343.9	0.00268	3.42	0.6370	0.045	4568.19	1.07	4571.84	1.00
EC-W7 &	4.1	0.6	0.3	302	10902.7	—	—	0.6250	0.021	4566.15	0.30	4566.14	0.30
EC-W8 &	44.2	0.8	0.8	1331	6953.1	0.000122	7.25	0.62538	0.0085	4565.63	0.14	4565.78	0.14
EC-R &	42.9	1.2	1.0	1366	16604.9	0.000039	21.3	0.62513	0.0085	4565.91	0.14	4565.96	0.14
<i>Standards</i>						$^{206}\text{Pb}/^{204}\text{Pb}$ <i>corr</i>	<i>2SD</i> [%]	$^{207}\text{Pb}/^{206}\text{Pb}$ <i>corr</i>	<i>2SD</i> [%]		<i>n</i>		
NBS 983													
- SEM setup 0.25 ppb						2762.5	1.29	0.071186	0.25		5		
- FC setup 1 ppb						2721.75	7.85	0.07124	0.60		10		
- literature ^a						2695.4	5.4	0.07120	0.06				
NBS 981													
- SEM setup 0.5 ppb						16.9437	0.26	0.91466	0.06		10		
- FC setup 1 ppb						16.9412	0.26	0.91475	0.06		14		
- literature ^b						16.9405	0.01	0.91475	-				

^a Catanzaro et al. (1968). ^b Abouchami et al. (2000). * measured using Faraday cup setup. & measured using SEM setup.

394 **Table 6:** Weighted average U isotope compositions of EC 002 bulk rock and pyroxene samples and of BCR-2 terrestrial basalt standard,
395 as well as repeat analyses of the IRMM 184 U isotope standard (Richter et al., 2010).

Sample	Mass [mg]	U [ng]	$^{238}\text{U}/^{235}\text{U}$	2σ	n	^{238}U intensity [V]
EC 002 Bulk rock	~120	15	137.819	0.007	2	12
EC 002 Px leachates	~160	5	137.766	0.027	2	2.5
BCR-2 a	11.8	20	137.797	0.017	2	15
BCR-2 b	2.9	5	137.815	0.046	2	4
IRMM 184			137.668	0.008	8	2.5 - 15

396

397 **Table 7:** Al-Mg data for EC 002 fractions.

Sample	$^{27}\text{Al}/^{24}\text{Mg}$	\pm	$\delta^{25}\text{Mg}$ [‰]	2SE	$\delta^{26}\text{Mg}^*$ [‰]	2SE	n
EC Px	0.98	0.05	-0.825	0.014	0.010	0.010	4
EC Bulk rock	1.05	0.18	-0.736	0.037	0.013	0.020	7
EC fines	3.45	0.17	-0.840	0.054	0.139	0.006	8
EC fsp2-4	6.33	0.32	-0.729	0.012	0.370	0.004	4
EC fsp1+8	9.03	0.45	-1.104	0.013	0.532	0.005	4
EC fsp7	10.7	0.54	-0.957	0.010	0.636	0.016	4
EC fsp6	34.4	1.72	-0.956	0.015	2.058	0.015	4

398

399 **Table 8:** Pb isotope data and corresponding Pb-Pb ages of merrillites analyzed by SIMS

Merrillites	²⁰⁷ Pb/ ²⁰⁴ Pb	±1s.e.	²⁰⁶ Pb/ ²⁰⁴ Pb	±1s.e.	²⁰⁷ Pb/ ²⁰⁶ Pb	±1s.e.	²⁰⁷ Pb/ ²⁰⁶ Pb corr [Ma] ^a	±1s.e.	²⁰⁷ Pb/ ²⁰⁶ Pb age [Ma] ^b	±1s.e.
M1	2368	352	3799	565	0.6245	0.0036	0.6226	0.0037	4561.0	8.6
M4	1738	191	2773	306	0.6243	0.0033	0.6226	0.0032	4560.9	7.5
M5	24360	8636	38710	13750	0.6271	0.0023	0.6268	0.0023	4570.7	5.2
M8-1	5252	889	8429	1426	0.6233	0.0027	0.6228	0.0025	4561.4	5.8
M8-2	8178	1597	13080	2554	0.6254	0.0032	0.6249	0.0032	4566.5	7.4
M12	5315	1474	8442	2342	0.6244	0.0048	0.6223	0.0044	4560.4	10.2
M14	2620	429	4164	682	0.6243	0.0038	0.6225	0.0036	4560.8	8.4
Weighed mean age ± 95% confidence interval (Ma)									4564.3 ± 5.2	

400 ^a ²⁰⁷Pb-²⁰⁶Pb corr. compositions are corrected from primordial Pb contribution. ^b ²⁰⁷Pb-²⁰⁶Pb ages are calculated using the ²³⁸U/²³⁵U=137.82 ± 0.01 of the measured

401 whole-rock composition of EC 002 and correlated errors between Pb and U isotopic measurements.

3.3 MC-ICP-MS Pb isotopic analysis

Lead isotope data for leachates and residue of a pyroxene fraction are presented in Table 5.

Leachates W7 and W8, as well as the residue, are highly radiogenic, with raw $^{206}\text{Pb}/^{204}\text{Pb}$ ratios ranging from 6953 to 16604. The first leachates (W1-3 to W5+6) have $^{206}\text{Pb}/^{204}\text{Pb}$ ratios in the range of 41 to 344, with a low sample-to-blank ratio of 131 for W5+6. The sample-to-blank ratios of the remaining leachates range from 1549 to 3808, with the exception of W7 at 302. In an “inverse” $^{204}\text{Pb}/^{206}\text{Pb}$ - $^{207}\text{Pb}/^{206}\text{Pb}$ space, the leachates and residues are significantly overdispersed (MSWD = 391). Nevertheless, they plot along a line projecting towards the point of terrestrial Pb as defined by the model of Stacey and Kramers (1975), indicating that the pyroxene in the sample is free of initial, primordial Pb (Fig. 3) and that the Pb isotope compositions of the leachates and residues are a mixture of only radiogenic Pb ($^{204}\text{Pb} = 0$) and terrestrial Pb. This has been previously observed in the angrites Sahara 99555 (Amelin, 2008a; Connelly et al., 2008) and NWA 1670 (Schiller et al., 2015), as well as some chondrules (Bollard et al., 2017).

A statistically meaningful isochron (probability of fit > 0.05) can be calculated using leachates W4, W7, W8 and the residue R, however, W7 is omitted due to its negative $^{204}\text{Pb}/^{206}\text{Pb}$ ratio after background- and blank-correction, despite it still plotting along the isochron. This leaves three fractions defining the isochron (MSWD = 3.3), resulting in an age of 4565.87 ± 0.30 Ma (2σ) (Fig. 4), calculated with the $^{238}\text{U}/^{235}\text{U}$ ratio 137.766 ± 0.027 , determined from the pyroxene fraction. All ages given include error propagation on the U isotope composition, except for individual $^{207}\text{Pb}^*/^{206}\text{Pb}^*$ model ages of the leachates and residue.

The $^{207}\text{Pb}^*/^{206}\text{Pb}^*$ model ages (Table 5), calculated from both initial Pb as represented by the Nantan troilite (Blichert-Toft et al., 2010) and the Stacey & Kramers (SK) point representing terrestrial Pb, show no age difference for a given highly radiogenic leachate or the residue, as they

425 plot close enough to the y-axis to not make any significant difference in y-intercept
426 ($= {}^{207}\text{Pb}^*/{}^{206}\text{Pb}^*$). The agreement between those leachates and the residue also demonstrates that
427 no fractionation occurred due to the use of HF in the leaching procedure. For the less radiogenic
428 leachate W4, the Nantan and SK model ages differ significantly, the SK model ages being in line
429 with the other leachates and residue of its respective fraction, indicating once again that there likely
430 was no primordial Pb present in the sample. The weighted average of the SK model ages for W4,
431 W8 and R results in an Pb-Pb age of 4565.87 ± 0.40 Ma (MSWD = 2.1). Adding the SK model
432 age for W7, where only its ${}^{207}\text{Pb}/{}^{206}\text{Pb}$ ratio is considered, to the weighted average gives an age of
433 4565.90 ± 0.36 Ma (MSWD = 1.7).

434

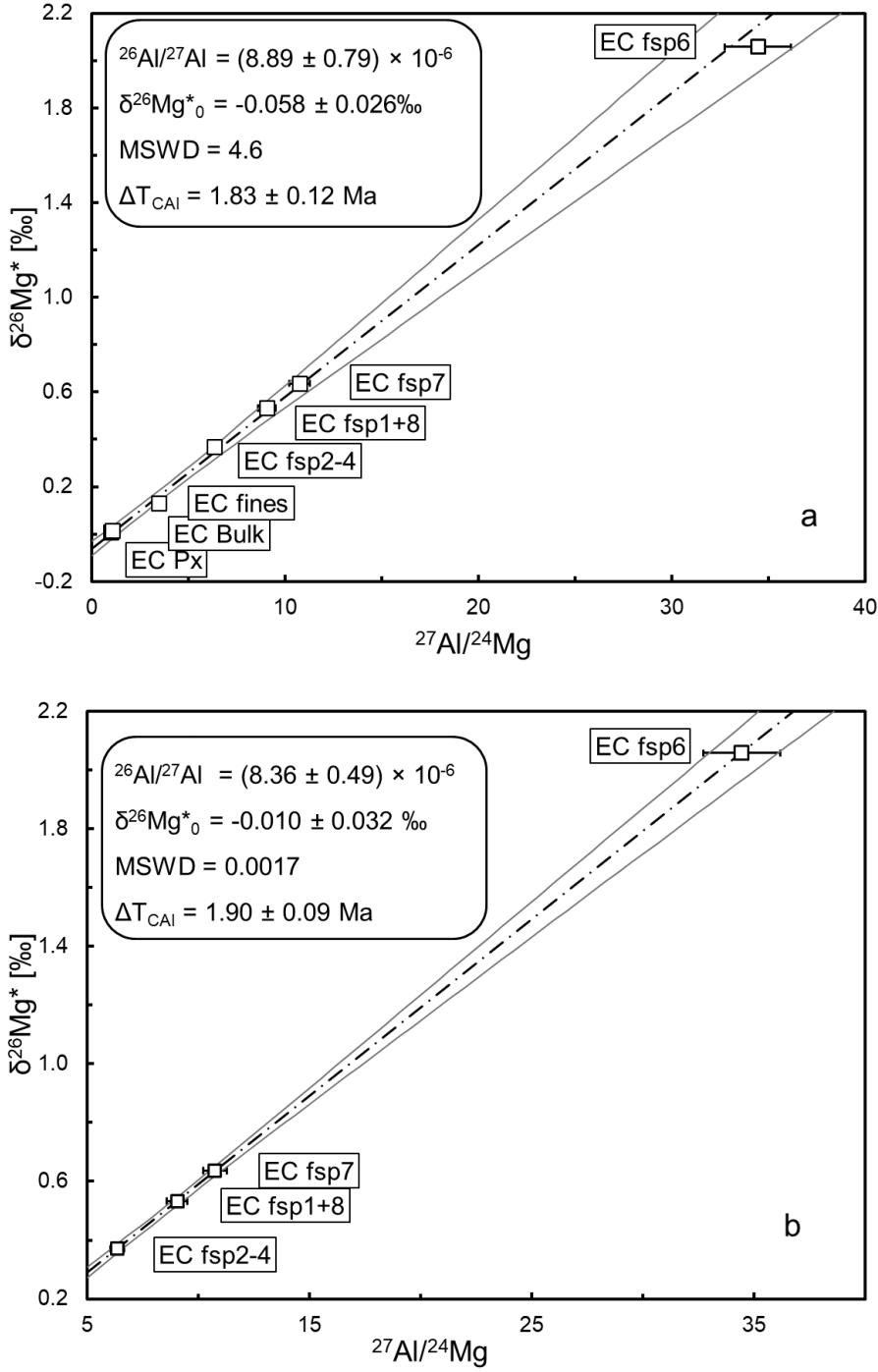


Figure 2: Internal ^{26}Al - ^{26}Mg isochrons defined by a) pyroxene, bulk rock, fine-grained and plagioclase fractions, corresponding to a $^{26}\text{Al}/^{27}\text{Al}$ ratio of $(8.89 \pm 0.79) \times 10^{-6}$ and a formation age of $1.83 \pm 0.12 \text{ Ma}$ after CAI formation, based on the canonical $^{26}\text{Al}/^{27}\text{Al}$ abundance (Jacobsen et

al., 2008); and **b)** only plagioclase fractions, corresponding $(8.36 \pm 0.49) \times 10^{-6}$ and a formation age of 1.90 ± 0.09 Ma after CAI formation. Uncertainties are 2SE errors on $\delta^{26}\text{Mg}^*$ measurements and $\pm 5\%$ on $^{27}\text{Al}/^{24}\text{Mg}$ ratios.

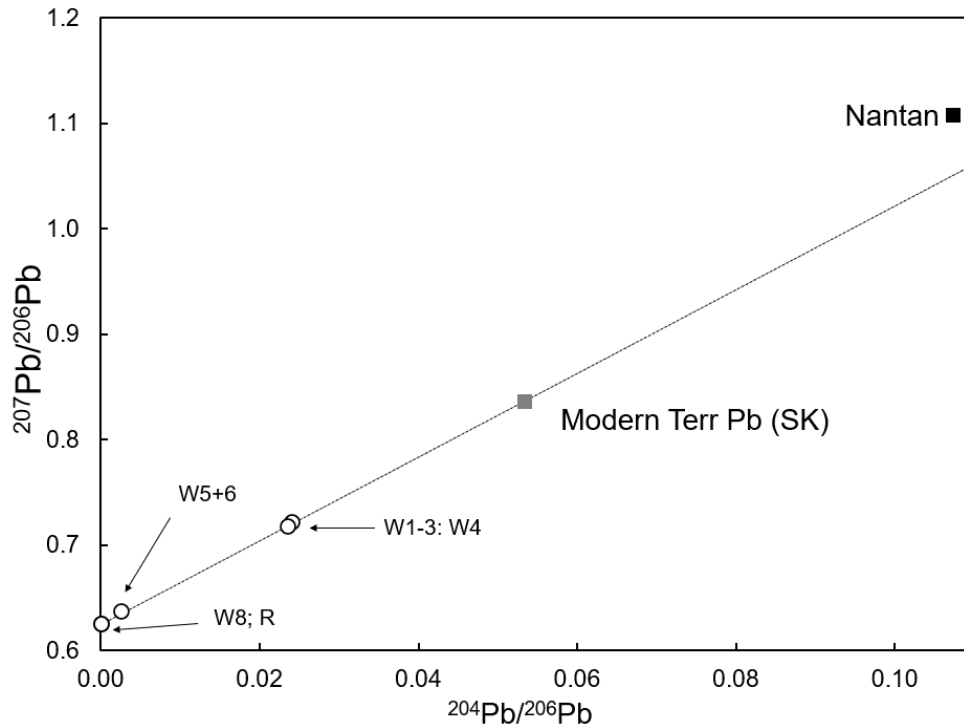


Figure 3: Regression line through the analyzed Pb fractions. Leachate W7 is omitted due to its negative blank-corrected $^{204}\text{Pb}/^{206}\text{Pb}$ ratio. Also plotted are data points for the Nantan troilite, representing the primordial Pb composition of the Solar System (Blichert-Toft et al., 2010), and the Stacey and Kramers (1975) data point representing the terrestrial Pb composition. Symbols of data points have been enlarged for clarity, larger than their uncertainties.

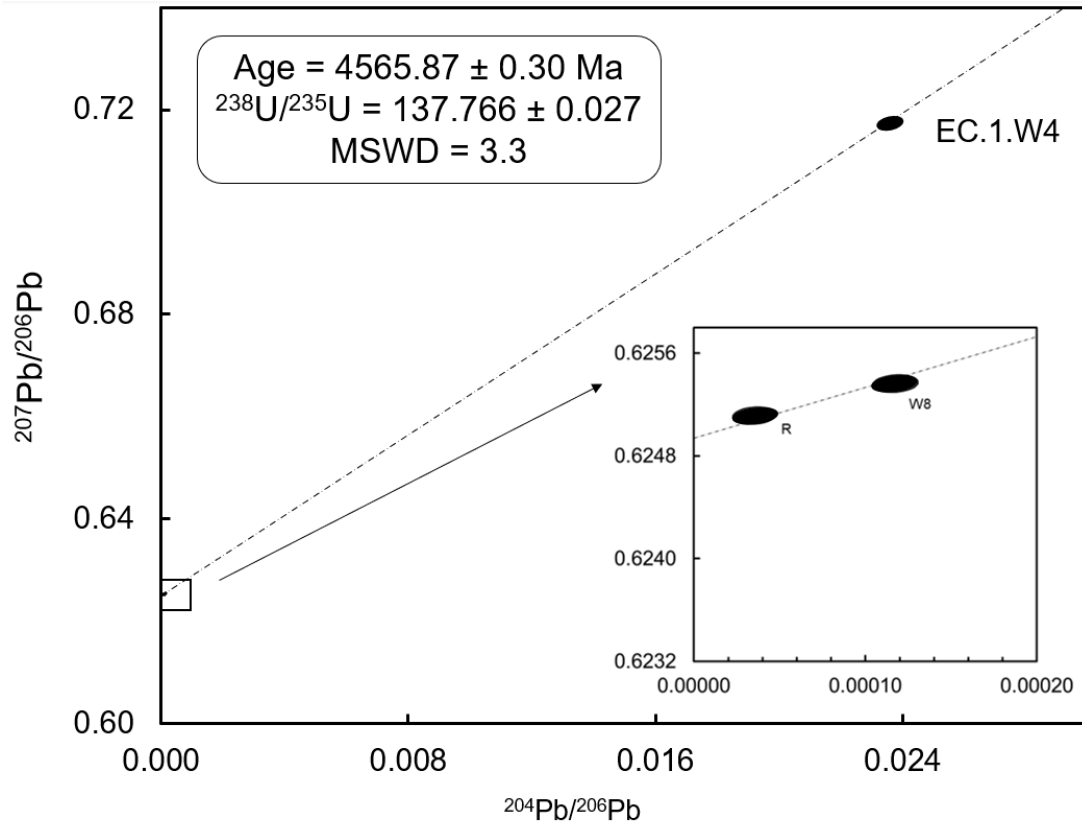


Figure 4: Inverse Pb-Pb isochron diagram for Erg Chech 002. The uncertainty on W4 is smaller than the ellipse, as it is enlarged for clarity. The inset shows the highly radiogenic leachate W8 and residue. Leachate W7 would plot along the regression line in negative $^{204}\text{Pb}/^{206}\text{Pb}$ vs. $^{207}\text{Pb}/^{206}\text{Pb}$ space.

3.4 Pb-Pb merrillite ages by SIMS

Merrillites have a homogeneous and H-free composition of $\text{Ca}_{8.5}\text{Na}_{0.8}\text{Mg}_{0.7}\text{Fe}_{0.3}(\text{PO}_4)_7$ ($n=4$). Raw Pb isotopic data were reduced and calibrated against measurements of standard Madagascar apatite (485 Myr, Thomson et al., 2012) using in-house-developed software (ZIPS version 3.1.1, by Christopher Coath). Common lead correction was made using the composition and model of Stacey and Kramers (1975) and primordial Pb isotopic composition reported for Canyon diablo

troilite by Tatsumoto et al. (1973). In the absence of suitable merrillite standard, U and Pb secondary ion yields were not known precisely, as such, U/Pb systematics cannot be measured with satisfactory precision. But if the analysed points were used as hypothetical standard, all results plotted tightly into a concordant cluster, strongly suggesting that the observed discrepancy derived chiefly from matrix effect (i.e., using apatite as standards for merrillite samples). Due to the extremely high radiogenic Pb isotopic ratios measured for merrillites in Erg Chech 002 (common lead $^{204}\text{Pb} < 0.1$ cps, and $^{204}\text{Pb}/^{206}\text{Pb}$ ratio on the order of 10^{-4} - 10^{-5}), the choice of the apatite standard (comparably aged apatite or merrillite standards are not available) as well as primordial Pb isotopic ratio did not affect the calculated Pb-Pb merrillite ages.

The seven ^{207}Pb - ^{206}Pb ages of individual analysis (Table 8) were calculated from radiogenic $^{207}\text{Pb}^*$ - $^{206}\text{Pb}^*$ ratio using the U decay constants from Steiger and Jäger (1977), with uncertainties of 0.2-0.4% ($\pm 2\sigma$), and a $^{238}\text{U}/^{235}\text{U}$ ratio of 137.82 ± 0.01 (from our whole-rock measurement). In the end, the ^{207}Pb - ^{206}Pb merrillite age for EC 002 was reported with a weighted mean of 4564.3 ± 5.2 Ma (2σ), as seen in Fig. 5.

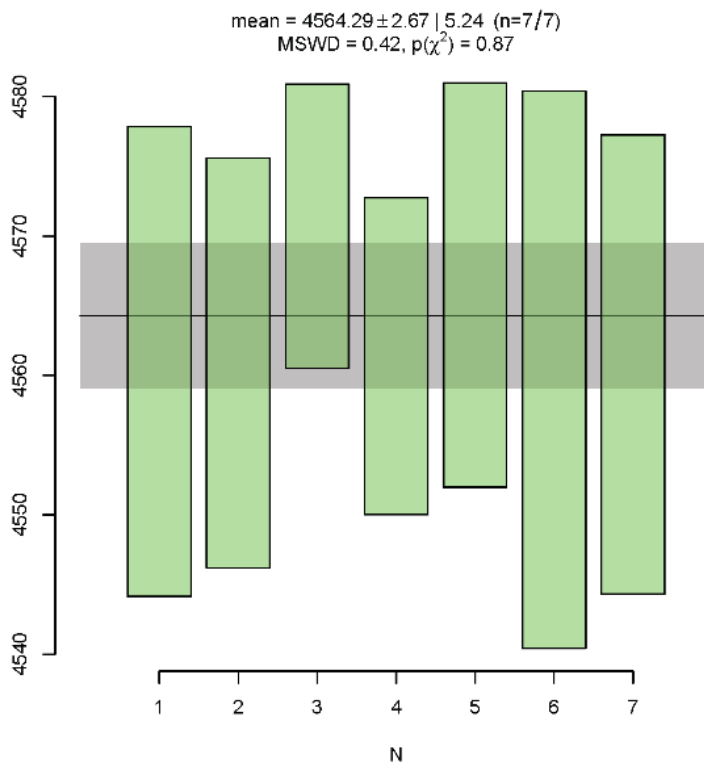


Figure 5: Weighted mean age in Ma with 1σ and 95% confidence interval for 7 spot analyses of 6 individual merrillite grains of EC 002 (Table 8).

4. Discussion

4.1 Lead isotope systematics

Even though only three fractions make up our ^{207}Pb - ^{206}Pb isochron, with a rather non-radiogenic leachate and a highly radiogenic leachate and residue, it is statistically meaningful (Pb-Pb age = 4565.87 ± 0.09 Ma, MSWD = 3.3, probability of fit = 0.068). Three-point isochrons are generally considered to be unreliable, as the regression may be subject to increased bias by outlying data points and data filtering. These concerns are valid, however, in this case, the highly radiogenic leachates used in the regression argue for the reliability of our age determined from the isochron:

Pb-Pb ages are determined by the intercept of the regression line with the y-axis in an “inverse” Pb-Pb diagram ($^{207}\text{Pb}^*/^{206}\text{Pb}^*$). In the case of EC 002, the later leachates and residue are highly radiogenic, defining a precise intercept, making any scatter of the less radiogenic leachates less influential on the Pb-Pb age. This is visible when including leachates that were not used in the final isochron and in the $^{207}\text{Pb}^*/^{206}\text{Pb}^*$ model ages. For example, including W5+6 instead of, or in addition to, W4 results in overdispersed errorchrons with an absolute age of 4565.78 ± 0.31 Ma (MSWD = 8.3) or 4565.91 ± 0.50 (MSWD = 27), respectively. In addition to this example, the weighted average of the $^{207}\text{Pb}^*/^{206}\text{Pb}^*$ SK model ages of the W4, W8 and R fractions (4565.87 ± 0.36 Ma, MSWD = 2.1) is consistent with the isochron age, as is the weighted average of the model ages when including the W7 leachate (4565.90 ± 0.40 Ma, MSWD = 1.7). Hence, we interpret the absolute age of 4565.87 ± 0.30 Ma as defined by the isochron as the crystallization age of EC 002 (Fig. 4).

Seven SIMS measurements of merrillites are consistent within errors and provide a weighted mean age of 4564.3 ± 5.2 Ma (2σ). While relatively much less precise than the age determination by solution analyses, this Ca-phosphate formation age is similar within uncertainty to the pyroxene Pb-Pb age. This reinforces the conclusions made by Barrat et al. (2021) suggesting a rapid cooling of the parent body. The diffusion rate of Pb in Ca-phosphate is faster than in pyroxene and therefore the closure temperature of the U-Pb system in phosphate is protracted toward lower temperatures (Cherniak, 2001) and more prone to resetting temperatures such as those sustained during impact events. This additional thermochronological information supports that EC 002 cooled rapidly after crystallization and was neither subjected to substantial impact events nor extensively thermally metamorphosed after ~ 4559 Ma. Detailed thermochronological records can be used to constrain EC 002’s parent body accretion history and size, and burial depth.

4.2 Uranium-corrected Pb-Pb age of Erg Chech 002

The $^{238}\text{U}/^{235}\text{U}$ ratio of bulk rock EC 002 is 137.819 ± 0.010 , distinct from the combined leachates (W5 to R) of the Px fractions at 137.766 ± 0.027 by 0.38 ± 0.21 ‰. The resulting U-corrected Pb-Pb ages are 4566.43 ± 0.14 Ma and 4565.87 ± 0.30 Ma, respectively, a difference of 0.56 ± 0.28 Myr. With that in mind, the choice of $^{238}\text{U}/^{235}\text{U}$ ratio for calculating the Pb-Pb age is an important consideration, as the interpretation of the result may change depending on which value is used. Since the Pb isotope systematics of EC 002 were determined on a pyroxene fraction of EC 002, we use the $^{238}\text{U}/^{235}\text{U}$ ratio of the same mineral fraction to calculate the U-corrected Pb-Pb age. The Pb-Pb ages in achondrites are usually determined from leachates and residues of pyroxene, which incorporate more U (e.g., Amelin, 2008b; Bouvier et al., 2011). The U isotope compositions of the same meteorites are however determined on unleached whole-rocks, sometimes from different laboratories (Brennecka and Wadhwa, 2012; Tissot et al., 2017). If U contamination in secondary minerals formed during desert weathering (e.g. carbonates, sulfates) or U isotope heterogeneity between pyroxenes and bulk rock samples exist in dated samples, U-corrected Pb-Pb ages would require further correction. Ideally, whenever Pb-Pb ages are determined from mineral fractions, so should the $^{238}\text{U}/^{235}\text{U}$ ratio. In practice, however, this is most often hampered by the large sample amounts necessary (> 100 mg) to ensure sufficient U to obtain a precise analysis. Analyzing the same mineral fractions for U and Pb isotopic compositions ensures consistency and avoids the assumption that there are no U isotope variations between pyroxene and bulk rock fractions of the sample or contribution from terrestrial U contamination or secondary minerals (e.g., carbonates) in whole-rock composition, which is a great concern for desert find meteorites.

The difference in $^{238}\text{U}/^{235}\text{U}$ ratio between the bulk rock and pyroxene fractions requires an explanation and could reasonably have originated through i) internal heterogeneities between minerals and the bulk rock sample; ii) fractionation during the acid-leaching procedure; or iii) fractionation during column chemistry and/or isotopic analysis.

The third possibility can be ruled out, as two BCR-2 aliquots underwent the same chromatographic and analytical procedures with comparable amounts of U as the two EC 002 samples without producing any evidence of fractionation within their statistical uncertainties (Table 6). These results also rule out any significant interference on mass 235 during analysis of small U amounts, as suggested by Connelly et al. (2019) to explain an outlier $^{238}\text{U}/^{235}\text{U}$ ratio in a troilite nodule of IVA meteorite Muonionalusta (Blichert-Toft et al., 2010).

Previously, Brennecka and Wadhwa (2012) reported a slightly lighter U isotope composition (by 0.30 ± 0.25 ‰) of the leachate fraction compared to the residue of the angrite NWA 6291, for which they invoked the removal of terrestrial components during leaching. Tissot et al. (2017), however, pointed out that the leachate contained ~ 64% of total U of the sample and that such an amount was unlikely to be exclusively of terrestrial origin, and instead argued for U isotope variability between pyroxene and phosphate, caused by magmatic differentiation, to explain different $^{238}\text{U}/^{235}\text{U}$ ratios between plutonic and volcanic angrites.

In the case of EC 002, the early leachates (W1 to W4) contain almost 80% of total U of the sample. Following the argumentation of Tissot et al. (2017), this suggests that the origin of the distinct $^{238}\text{U}/^{235}\text{U}$ ratios is isotopic heterogeneity between pyroxene and any remaining minerals. The acid-leaching procedure should not have affected the U isotope composition of the pyroxene, as the acids used in the early leaching steps (0.5 M HBr, water, 0.5 M HNO_3 and 6 M HCl; Table 3), whose leachates were not included in the analyzed fraction, do not dissolve pyroxene. Rather, they

dissolve feldspar, phosphates, troilite, as well as any potential secondary terrestrial components, that may have remained attached to pyroxene grains after hand-picking (Bouvier et al., 2005; Ito et al., 2019). Therefore, the U isotope composition of the “re-combined residue” consisting of leachates W5-8 and the residue from the leaching procedure should represent the true $^{238}\text{U}/^{235}\text{U}$ ratio of the EC 002 pyroxene megacrysts, free of other mineral or terrestrial contamination.

Based on this, a mass balance calculation estimates a $^{238}\text{U}/^{235}\text{U}$ ratio of ~ 137.83 for the removed components (re-combined W1 to W4 leachates), a difference of up to $\sim 0.45\%$. This is larger than observed in NWA 6291 (Brennecka and Wadhwa, 2012), but comparable to results reported in a conference abstract by Huyskens et al. (2020) between merrillite and the bulk rock fraction in the plutonic angrite Angra dos Reis.

These results show that the bulk rock U isotope composition may not be wholly representative for age correcting pyroxene fractions using Pb-Pb chronometry. Age corrections may be necessary to account for potential isotopic heterogeneities between pyroxene and bulk rock fractions of certain achondrites. This discussion re-emphasizes the need for more detailed and systematic investigations into the U isotope compositions of achondrites and their minerals, but also the effect that acid leaching potentially has on them.

4.3 ^{26}Al - ^{26}Mg systematics

Regressing the ^{26}Al - ^{26}Mg data from seven fractions of EC 002 results in an isochron with excess scatter (MSWD = 4.6) and a crystallization age of 1.83 ± 0.12 Ma after CAI formation (Fig. 2a).

The four plagioclase fractions of our dataset define an isochron with an age of 1.90 ± 0.09 Ma after

580 CAI formation, identical within the stated uncertainties but with no excess scatter (MSWD =
 581 0.002; Fig. 2b). When anchored to the absolute age of CAIs (4567.30 ± 0.16 ; Connelly et al.,
 582 2012), they result in absolute ages of 4565.47 ± 0.20 Ma and 4565.40 ± 0.18 Ma, respectively. The
 583 excess scatter of the regression through all fractions is likely the result of the presence of accessory
 584 phases in the fines fraction, and/or xenolithic material in the bulk rock and pyroxene fractions (e.g.,
 585 Barrat et al., 2021, Nicklas et al, 2022). The plagioclase-only isochron is less likely to be affected
 586 by xenolithic material, which could explain the low MSWD. The difference is not resolvable at
 587 this level of precision, therefore for chronological purposes we conservatively use the isochron
 588 that includes all fractions (1.83 ± 0.12 Ma after CAI formation) going forward.
 589 The crystallization age of 1.83 ± 0.12 Ma after CAI formation is consistent with, albeit less precise
 590 than the age of 1.83 ± 0.04 Ma determined by Fang et al. (2022). Both these ages are respectively
 591 0.46 ± 0.13 and 0.46 ± 0.05 Myr older than the ^{26}Al - ^{26}Mg age of 2.29 ± 0.04 Ma after CAI
 592 formation (both re-calculated with a ^{26}Al half-life of 0.717 Myr) reported by Barrat et al. (2021),
 593 which was determined by SIMS (Fig. 6). Our age is strengthened by the analysis of different
 594 plagioclase fractions with a good spread in $^{27}\text{Al}/^{24}\text{Mg}$ ratios, and with that subset of our data in
 595 agreement with our overall isochron. The differences of these results to those of Barrat et al. (2021)
 596 have also been discussed by both Fang et al. (2022) and Zhu et al. (2022). Potentially, when
 597 analyzing sample spots with very low amounts of Mg by SIMS, such as those with $^{27}\text{Al}/^{24}\text{Mg}$ ratios
 598 between 2000 and 5000, matrix effects have to be strongly considered when using in-situ analytical
 599 methods and counting statistics errors could become a factor, where background corrections could
 600 hypothetically overcorrect the amount of Mg isotopes, leading to spuriously low ^{26}Mg excesses.
 601 Furthermore, the calibrating standard used, Miyake-Jima plagioclase, has a $^{27}\text{Al}/^{24}\text{Mg}$ ratio of

396.3, an order of magnitude lower than the plagioclase analyzed in their sample of EC 002, which could lead to miscalibration for the measurements with higher $^{27}\text{Al}/^{24}\text{Mg}$ ratios (Zhu et al., 2022). An alternative interpretation is that the isochron determined by Barrat et al. (2021) represents the time of closure of pure plagioclase ($^{27}\text{Al}/^{24}\text{Mg} > 1500$), whereas our isochron with fractions that contain at least some proportion of other minerals represents the time of closure of a mineral mixture with a higher closure temperature for Mg diffusion. Closure temperatures of pyroxene and anorthite have been estimated at 900°C to 1000°C and 700°C to 800°C, respectively (Wadhwa et al., 2009). With the age difference of 0.46 ± 0.13 Myr between isochrons, based on those closure temperatures as an upper limit, the cooling rate would be 465°C/Myr, several orders of magnitude slower than what Barrat et al. (2021) estimated from the petrology of EC 002 (5°C/yr from 1200°C to 1000°C, and >0.1 to 1°C/day below 900°C). Such a large difference cannot be explained by the isochrons representing different times of closure of minerals and still satisfy the petrological constraints established on the cooling rate of EC 002. Fang et al. (2022) argued similarly that the plagioclase cores analyzed by the SIMS ion probe were not a closed system for Mg diffusion. The younger SIMS ^{26}Al - ^{26}Mg age (Barrat et al., 2021) may be the result of the resumption of Mg diffusion due to a re-heating event above the closure temperature in plagioclase.

In addition, the $\delta^{26}\text{Mg}^*_0$ values (initial $^{26}\text{Mg}/^{24}\text{Mg}$ ratio) between our study, Barrat et al. (2021) and Fang et al. (2022) are distinct (Fig. 7). Barrat et al. (2021) first reported the $\delta^{26}\text{Mg}^*_0$ of 0.065 ± 0.085 ‰, followed by the -0.009 ± 0.005 ‰ of Fang et al. (2022). The $\delta^{26}\text{Mg}^*_0$ for our regression through all fractions is -0.058 ± 0.026 ‰, distinctly lower than both previous studies. The $\delta^{26}\text{Mg}^*_0$ of the regression through the plagioclase fractions only is -0.010 ± 0.032 ‰, which is similar to the initial value of Fang et al. (2022). Our two initial values are less precise than the one reported by Fang et al. (2022) due to the absence of data points with $^{27}\text{Al}/^{24}\text{Mg}$ ratios < 0.9 , but more precise

625 from the higher value reported by Barrat et al. (2021). The difference between the all-fraction and
 626 plagioclase-only isochron may be attributed to earlier-formed xenolithic material affecting the bulk
 627 rock and pyroxene fractions. The $\delta^{26}\text{Mg}^*_0$ of -0.058 ± 0.026 ‰, while within uncertainty of the
 628 “canonical” initial Solar System value (-0.034 ‰; Jacobsen et al., 2008; Schiller et al., 2010),
 629 would require crystallization coeval with the formation of CAIs, which is inconsistent with all
 630 reported ^{26}Al - ^{26}Mg ages. Some studies have reported “sub-canonical” initial $\delta^{26}\text{Mg}^*_0$ values up to
 631 -0.128 ‰ in otherwise “canonical” CAIs (Wasserburg et al., 2012; MacPherson et al., 2017),
 632 arguing for $\delta^{26}\text{Mg}^*_0$ heterogeneity in the early Solar System. While this could explain the low
 633 $\delta^{26}\text{Mg}^*_0$ of -0.058 ± 0.026 ‰, there is no evidence for this in other Al-Mg studies of chondrites
 634 and achondrites. Part of this discrepancy in $\delta^{26}\text{Mg}^*_0$ values reported so far is that both Barrat et al.
 635 (2021) and Fang et al. (2022) calculated the mass-independent $\delta^{26}\text{Mg}^*$ values using the
 636 equilibrium fractionation factor ($\beta = 0.521$). For EC 002, which is a rapidly cooled sample, we
 637 argue that kinetic mass fractionation ($\beta = 0.511$) more appropriately models Mg isotope
 638 fractionation, as equilibrium mass fractionation is negligible under these conditions (Teng et al.,
 639 2007). This is further supported by the mass-dependent fractionation of our rock standard data of
 640 the San Carlos olivine and CV3 chondrite Allende (Figs. S1 and S2). As Fang et al. (2022) did not
 641 publish the stable Mg isotope compositions of their mineral fractions, their $\delta^{26}\text{Mg}^*$ values cannot
 642 be re-calculated with the kinetic fractionation factor to estimate the effect of fractionation factor.
 643 Re-calculating the data from Barrat et al. (2021) with the kinetic fractionation factor results in a
 644 $\delta^{26}\text{Mg}^*_0$ value of 0.024 ± 0.055 ‰. This is closer to the value of Fang et al. (2022) and our
 645 plagioclase-only isochron, indicating a likely better approximation of the true $\delta^{26}\text{Mg}^*_0$ value of
 646 EC 002. For completeness, using the equilibrium fractionation factor instead shifts the $\delta^{26}\text{Mg}^*_0$

values of our isochrons even lower to -0.086 ± 0.035 ‰ and -0.037 ± 0.032 ‰ for the full and plagioclase-only isochron, respectively.

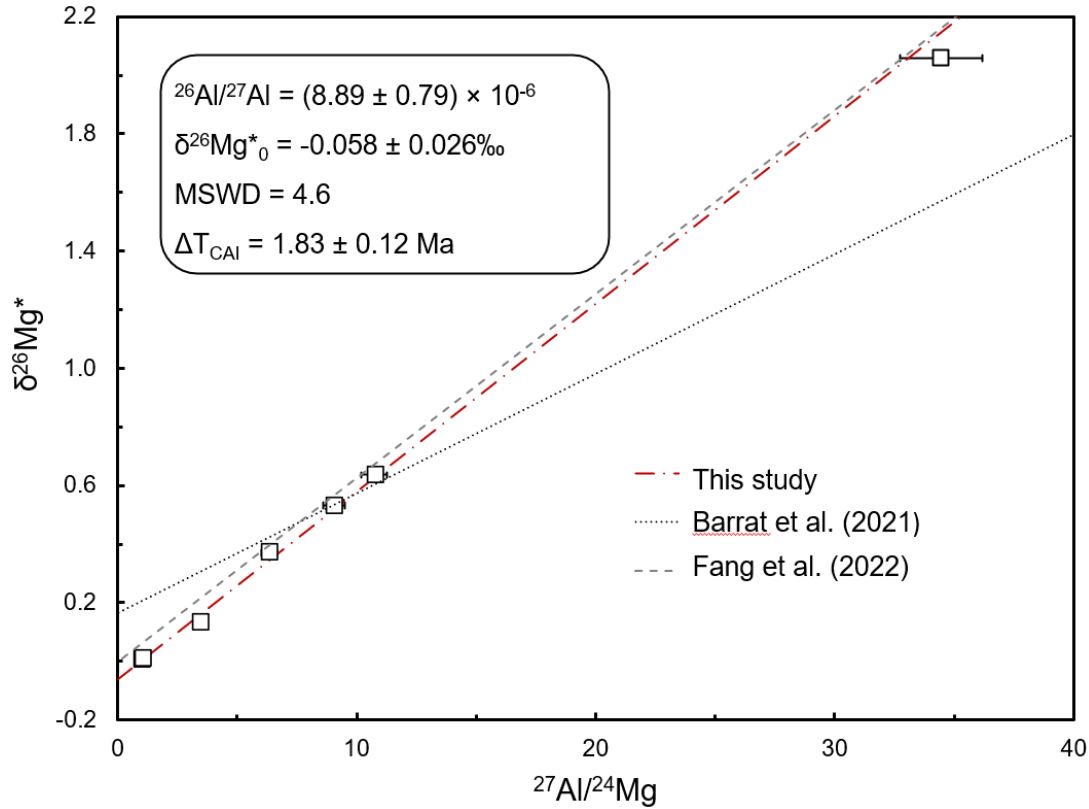


Figure 6: Comparison of initial $^{26}\text{Al}/^{27}\text{Al}$ ratios between this study, Fang et al. (2022) and Barrat et al. (2021). Error envelopes of isochrons have been omitted for clarity.

The $\delta^{25}\text{Mg}$ mass-dependent values of the analyzed mineral fractions are isotopically light compared to terrestrial rocks, bulk chondrites and other achondrites (e.g., Sedaghatpour and Teng, 2016). Due to the absence of reported mass-dependent Mg isotope data by Fang et al. (2022), we cannot compare our data to this other study of EC 002. Standards that underwent analysis and the same Mg separation procedure as the one employed for samples are consistent with their reported compositions (Table 1). Any process to fractionate Mg isotopes would therefore have had to occur

between crystallization and dissolution of the samples. Terrestrial alteration may be a possibility. EC 002 shows signs of oxidation and secondary weathering products (Gattaccecca et al., 2021), but terrestrial weathering should cause an enrichment in heavier Mg isotopes, not a depletion (Teng et al., 2010). While the exact provenance of these light $\delta^{25}\text{Mg}$ values is unknown, the good agreement of the initial $^{26}\text{Al}/^{27}\text{Al}$ ratio with Fang et al. (2022) suggests that the responsible process, be it natural or analytical, did not affect the mass-independent values nor the ^{26}Al - ^{26}Mg chronometry.

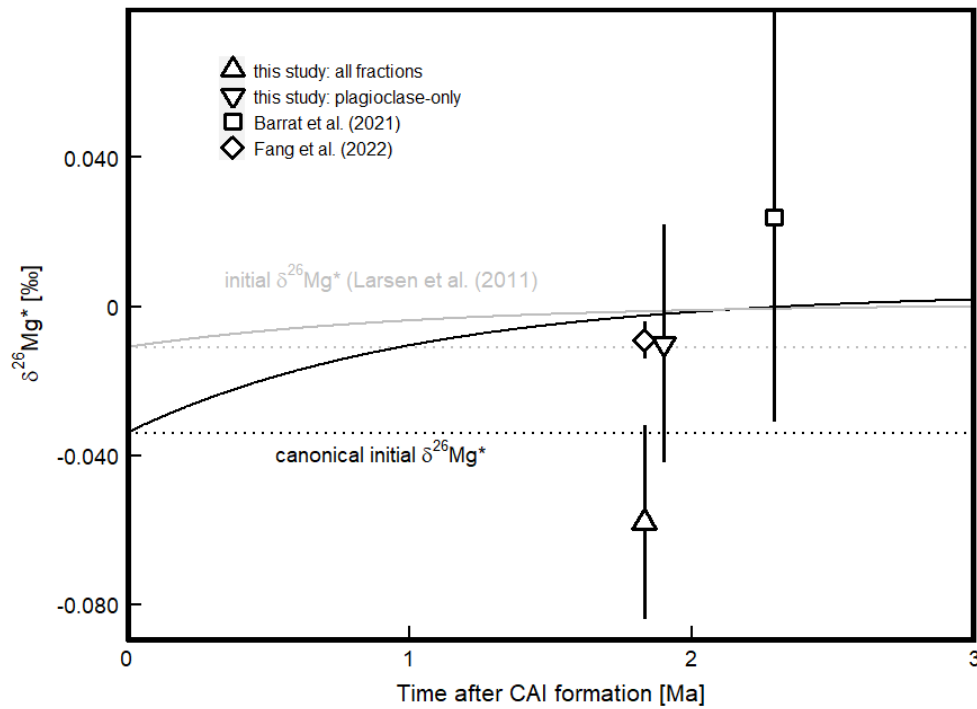


Figure 7: Presentation of the different $\delta^{26}\text{Mg}^*_0$ values of Barrat et al. (2021), Fang et al. (2022), as well as our isochron containing all fractions and the isochron containing only plagioclase fractions. Plotted alongside are the $\delta^{26}\text{Mg}^*$ evolution lines assuming canonical and sub-canonical $^{26}\text{Al}/^{27}\text{Al}$ ratios and $\delta^{26}\text{Mg}^*_0$ values (5.23×10^{-5} , -0.034 ‰: Jacobsen et al., 2008; 1.6×10^{-5} , -0.016 ‰: Larsen et al., 2011).

4.4 Combined short-lived chronology and U-corrected Pb-Pb ages

Time anchors are used to calculate absolute model ages of samples that were dated by short-lived chronometers. To anchor relative ^{26}Al - ^{26}Mg to absolute ages, analyzed samples are most commonly anchored to the absolute age of CAIs (4567.30 ± 0.16 Ma; Connelly et al., 2012). Some achondrites have also been proposed and used as anchors, such as the angrite D'Orbigny, particularly for the ^{53}Mn - ^{53}Cr chronometer due to the lack of Mn in CAIs (e.g., Glavin et al., 2004; Wadhwa et al., 2009; Sanborn et al., 2019).

The distribution and abundance of the parent nuclide at time of formation between individual meteorites as well as meteorite formation reservoirs can be then made. For example, previous studies of angrites has suggested that the initial $^{26}\text{Al}/^{27}\text{Al}$ of the inner Solar System (NC reservoir) was $\sim 1 \times 10^{-5}$, significantly lower than the accepted “canonical” value ($\sim 5 \times 10^{-5}$) determined from CAIs (Schiller et al., 2015). This was based on a discrepancy of ~ 1 to 2 Myr between Pb-Pb ages and ^{26}Al - ^{26}Mg ages of the angrites when anchored to CAIs. They posit that the inner Solar System (NC reservoir) was depleted in ^{26}Al through thermal processing due to it being closer to the proto-Sun (Schiller et al., 2018), before CI-like, ^{26}Al -enriched dust was admixed to that formation reservoir (Bollard et al., 2019). To further investigate this hypothesis, we anchor ^{26}Al - ^{26}Mg ages of different NC and CC achondrites to the absolute age of EC 002 as determined by our U-corrected Pb-Pb chronology. The early formation, rapid cooling history and undisturbed history of EC 002 (Barrat et al., 2021) make it a suitable candidate as an anchor meteorite.

The recent reporting of the Cr isotope systematics of EC 002 (negative bulk $\epsilon^{54}\text{Cr}$ values; Anand et al., 2022; Zhu et al., 2022) combined with O isotope data (Anand et al., 2022; Gattacceca et al., 2021) and negative Tm* anomaly (Barrat et al., 2021) indicate that EC 002 formed in the NC

reservoir, near the angrites, brachinites and HEDs. Therefore, its parent body should have formed
 with the same ^{26}Al abundance as the angrite parent body. This can be easily examined by anchoring
 the ^{26}Al - ^{26}Mg ages of three angrites (D'Orbigny, Sahara 99555 and NWA 1670) to EC 002. These
 three angrites also have published Pb-Pb ages, though the $^{238}\text{U}/^{235}\text{U}$ ratio of NWA 1670 has not
 been analyzed (Schiller et al., 2015), so that any potential discrepancies between the ^{26}Al - ^{26}Mg
 and U-corrected Pb-Pb chronometers can be examined. The resulting ^{26}Al - ^{26}Mg ages are visualized
 in Fig. 8 and listed in Table S3. To summarize, the U-corrected Pb-Pb age of D'Orbigny, Sahara
 99555 and NWA 1670 are systematically older by ~ 0.5 to 1.5 Myr than their ^{26}Al - ^{26}Mg ages
 anchored to EC 002. This suggests that ^{26}Al heterogeneity is not the underlying cause of these age
 discrepancies, but rather that there is some chronological disturbance in the angrites. This has been
 previously discussed based on apparent isotopic disturbances of Sm-Nd systematics in D'Orbigny
 (Sanborn et al., 2015). Furthermore, Sahara 99555 exhibits evidence of terrestrial alteration (e.g.,
 Floss et al., 2003) and potential re-distribution of Pb on the mineral grain scale (Amelin, 2008a),
 and NWA 1670 may have been shocked (Keil, 2012 and references therein), all of which could
 have affected the accuracy of the radiometric systems. Evidence for post-crystallization Mg
 isotope re-equilibration in plagioclase has also been observed in the NC ungrouped achondrite
 Asuka 881394 (Nyquist et al., 2003; Wadhwa et al., 2009; Hublet et al., 2017; Wimpenny et al.,
 2019), which shares a similar age discrepancy when anchored to EC 002 (Fig. 8, Table S3).
 In contrast to the angrites and Asuka 881394, the ^{26}Al - ^{26}Mg ages (anchored to EC 002) of the
 two ungrouped carbonaceous achondrites NWA 2976 and NWA 6704 are concordant to their U-
 corrected Pb-Pb ages (Fig. 8, Table S3: Schiller et al., 2010a; Bouvier et al., 2011b). This implies
 that, within the resolution of the chronometers, there were no significant variations of the ^{26}Al
 abundance between the NC (EC 002) and CC reservoir (NWA 2976 and NWA 6704).

In addition, it is important to note that using the U-corrected Pb-Pb age with the bulk rock $^{238}\text{U}/^{235}\text{U}$ ratio of 137.819 ± 0.010 and the corresponding older age of 4566.43 ± 0.14 Ma does not significantly alter the interpretation of these findings. Of the three angrites, the ^{26}Al - ^{26}Mg age of D'Orbigny (when anchored to EC 002) becomes concordant with its U-corrected Pb-Pb age. Those of NWA 1670 and also Sahara 99555, when using the more precise ^{26}Al - ^{26}Mg data of Schiller et al. (2015), still are over 0.5 Myr younger than their U-corrected Pb-Pb ages. Crucially, both the ^{26}Al - ^{26}Mg ages of the two ungrouped carbonaceous achondrites NWA 2976 and NWA 6704 remain concordant with their U-corrected Pb-Pb ages (Table S3). All these pieces of evidence do not suggest that ^{26}Al was distinctly different between the NC and CC reservoirs, and that ^{26}Al heterogeneities are not the cause of discordant ages between the ^{26}Al - ^{26}Mg and U-corrected Pb-Pb chronometers.

One remaining issue between the ^{26}Al - ^{26}Mg and U-corrected Pb-Pb ages of EC 002 is their own discordance when anchored to the absolute age of CAIs. The age difference between the U-corrected Pb-Pb age and the ^{26}Al - ^{26}Mg age of EC 002 is 0.40 ± 0.36 Myr (our data) or 0.40 ± 0.34 Myr (Fang et al., 2022). This results in $^{26}\text{Al}/^{27}\text{Al}$ ratios at the time of CAI formation of $[3.54^{+1.82}/_{-1.22}] \times 10^{-5}$ and $[3.54^{+1.43}/_{-1.03}] \times 10^{-5}$, respectively. These values appear lower than the “canonical” $^{26}\text{Al}/^{27}\text{Al}$ ratio, though both are within uncertainty of at least some internal isochrons of CAIs that also have old Pb-Pb ages (e.g., Jacobsen et al., 2008; Bouvier and Wadhwa, 2010). Both values, however, are clearly higher than the suggested $^{26}\text{Al}/^{27}\text{Al}$ ratio of the angrite parent body (APB) at time of CAI formation ($[1.33^{+0.21}/_{-0.18}] \times 10^{-5}$; Schiller et al., 2015). These age differences could be resolved by invoking earlier formation of CAIs at ~ 4567.7 Ma. The timing and duration of CAI formation has been discussed largely by previous workers (Bouvier and Wadhwa, 2010; Bouvier et al., 2011a; Sanborn et al., 2019; Wimpenny et al., 2019) and is beyond the scope of this study.

The most recent U-corrected absolute Pb-Pb age of CAIs (4567.30 ± 0.16 Ma; Connelly et al., 2012) is based on a weighted mean of four CAIs from the CV3 chondrites Efremovka and Allende (Amelin 2010, Connelly et al., 2012), both of which underwent aqueous alteration that may have re-distributed isotopes and disturbed the Pb-Pb systematics (e.g., Bouvier and Wadhwa, 2010; Krot et al., 2021). The initial $^{26}\text{Al}/^{27}\text{Al}$ ratios of those four CAIs have also not been determined *in situ* by SIMS, thereby not confirming if they actually formed with a “canonical” $^{26}\text{Al}/^{27}\text{Al}$ ratio.

Furthermore, there have been reports of older U/Th or U-corrected Pb-Pb ages of two CAIs, 2364-B1 from the CV3 chondrite NWA 2364 (Bouvier and Wadhwa, 2010) and 6991-B4 from the CV3 chondrite NWA 6991 (although not peer-reviewed, Bouvier et al., 2011a), with absolute Pb-Pb ages of $4568.2 (^{+0.2}_{-0.4})$ Ma and 4567.94 ± 0.31 Ma, respectively. Both D’Orbigny and NWA 6704 are concordant when anchored to the 2364-B1 CAI age, in contrast to the Efremovka + Allende CAIs (Sanborn et al., 2019). The U isotope composition of CAI 2364-B1 was not measured but estimated using the low measured Th/U ratio of the sample. Bouvier and Wadhwa (2010) used the correlation found between U/Th with $^{238}\text{U}/^{235}\text{U}$ (Brennecka et al., 2010) to propose an adjustment of up to -0.3 Myr to the internal mineral separate Pb-Pb age of the 2364-B1 CAI. The 2364-B1 U/Th-corrected Pb-Pb age is therefore consistent with the U-corrected 6991-B4 Pb-Pb age. The correlation between U/Th ratios and U isotopic compositions in CAIs was confirmed by Tissot et al. (2016) as produced by the decay of short-lived ^{247}Cm . The CAIs measured by two other studies did not fall on this correlation (Amelin et al., 2010; Connelly et al., 2012). Therefore, those samples did not support this proxy for correcting Pb-Pb ages of CAIs. The process responsible for such U isotopic variations in CAIs (beside from ^{247}Cm decay) is unknown.

The U and Al-Mg isotope compositions of NWA 6991 compact type A CAI (called B4) were measured (Bouvier et al., 2011a), but these data have not been published in a peer-reviewed

journal and remain available only in an abstract form. A protracted formation interval of CAIs of up to 0.4 Myr, as suggested by Kawasaki et al. (2019, 2020), based on *in situ* ^{26}Al - ^{26}Mg dating, could potentially resolve the differences in absolute ages. This would, however, still require investigation into the absolute timing of such CAIs, and not necessarily impact the age of the oldest CAIs that define the initial $^{26}\text{Al}/^{27}\text{Al}$ ratio in the Solar System. As it currently stands, the age of 4567.30 ± 0.16 Ma (Connelly et al., 2012) remains the most robust U-corrected Pb-Pb age for a CAI. Nevertheless, renewed attention to U-corrected Pb-Pb ages combined with Al-Mg systematics of CAIs from more pristine chondrites may be warranted.

Two recent studies aimed to determine the initial $^{53}\text{Mn}/^{55}\text{Mn}$ ratio of EC 002 to calculate its formation age using the ^{53}Mn - ^{53}Cr chronometer (Zhu et al., 2022; Anand et al., 2022). Notably, the results of the two studies do not agree with each other (Fig. 9, Table S3). Zhu et al. (2022) determined an initial $^{53}\text{Mn}/^{55}\text{Mn}$ ratio of $[5.85 \pm 0.45] \times 10^{-6}$ from an isochron based on various mineral fractions, resulting in an absolute age of 4566.66 ± 0.56 Ma when anchored to D'Orbigny. Conversely, the initial $^{53}\text{Mn}/^{55}\text{Mn}$ ratio of $[4.76 \pm 0.39] \times 10^{-6}$, determined by Anand et al. (2022) from leachates as well as a whole-rock, silicate and chromite fractions, results in an absolute age of 4565.56 ± 0.59 Ma, therefore younger by 1.10 ± 0.95 Myr than the study by Zhu et al. (2022). Anand et al. (2022) argue that the older age of Zhu et al. (2022) stems from higher fractions of xenolithic material within their sample set, as evidenced by larger $\epsilon^{54}\text{Cr}$ variations in them. While a sample like EC 002 is susceptible to heterogeneities between samples due to the presence of large megacrysts, it is questionable that this would result in an age difference as large as ~ 1 Myr. We note that Zhu et al. (2022) excluded xenolithic fractions (based on their $\epsilon^{54}\text{Cr}$ values) from their isochron. Certainly, these incongruent results warrant further measurements.

Regardless of the cause of these different ages, the chronological repercussions of the 1 Myr gap are substantial: the younger age obtained by Anand et al. (2022) is consistent with the U-corrected Pb-Pb age of EC 002, and with the ^{26}Al - ^{26}Mg ages anchored to CAIs (this study; Fang et al., 2022). Furthermore, the ^{53}Mn - ^{53}Cr ages of the three angrites D'Orbigny, NWA 1670 and Sahara 99555 (Glavin et al., 2004; Sugiura et al., 2005), NC achondrite Asuka 881394 (Wimpenny et al., 2019) and CC achondrite NWA 6704 (Sanborn et al., 2019), when anchored to the U-corrected Pb-Pb age of EC 002 are all concordant within the resolution of the chronometers. This result contrasts with the older ^{53}Mn - ^{53}Cr age by Zhu et al. (2022), to which none of the above achondrites are concordant (Fig. 10, Table S3). Given this context, it would seem that the initial $^{53}\text{Mn}/^{55}\text{Mn}$ ratio of $[4.76 \pm 0.39] \times 10^{-6}$ (Anand et al., 2022) may be more representative of EC 002. The concordance between ^{53}Mn - ^{53}Cr ages and U-corrected Pb-Pb ages when anchored to EC 002 with that particular value furthermore suggests that the ^{53}Mn - ^{53}Cr chronometer was not disturbed in Asuka 881394 and the angrites, in comparison with the ^{26}Al - ^{26}Mg chronometer. This would imply that the cause of chronological disturbance in those samples is due to Mg diffusion in plagioclase through later thermal events, rather than a more general re-setting of the chronometers. For ^{26}Al - ^{26}Mg chronometry, D'Orbigny should be avoided as an anchor based on these findings.

In summary, the age gap between U-corrected Pb-Pb and ^{26}Al - ^{26}Mg ages (when anchored to CAIs) in some angrites and Asuka 881394 is most likely to be attributed to later re-setting of the ^{26}Al - ^{26}Mg chronometer. Alternatively, U-corrected Pb-Pb ages of CAIs from the Efremovka and Allende meteorites that may have been affected by secondary alteration, resulting in spuriously young Pb-Pb ages. Heterogeneous $^{238}\text{U}/^{235}\text{U}$ ratios in bulk meteorites, as evidenced in pyroxene separates of EC 002, may contribute to age shifts of up to ~ 0.5 Myr, but are unlikely the main cause of age discordances of up to 2 Myr. Further advances in the analytical precision of both U

and Pb isotope measurements could potentially reveal more and/or larger differences in ages between the ^{26}Al - ^{26}Mg and Pb-Pb chronometers, indicating smaller scale chronological disturbances or secondary processes in meteorite parent bodies.

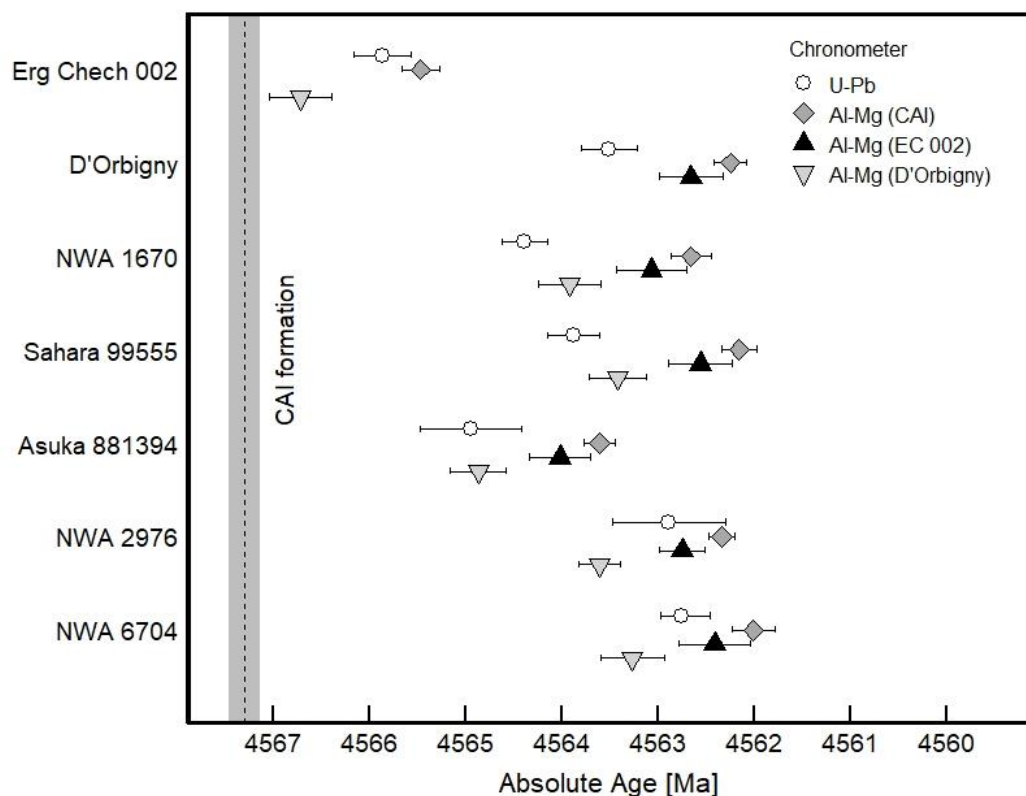
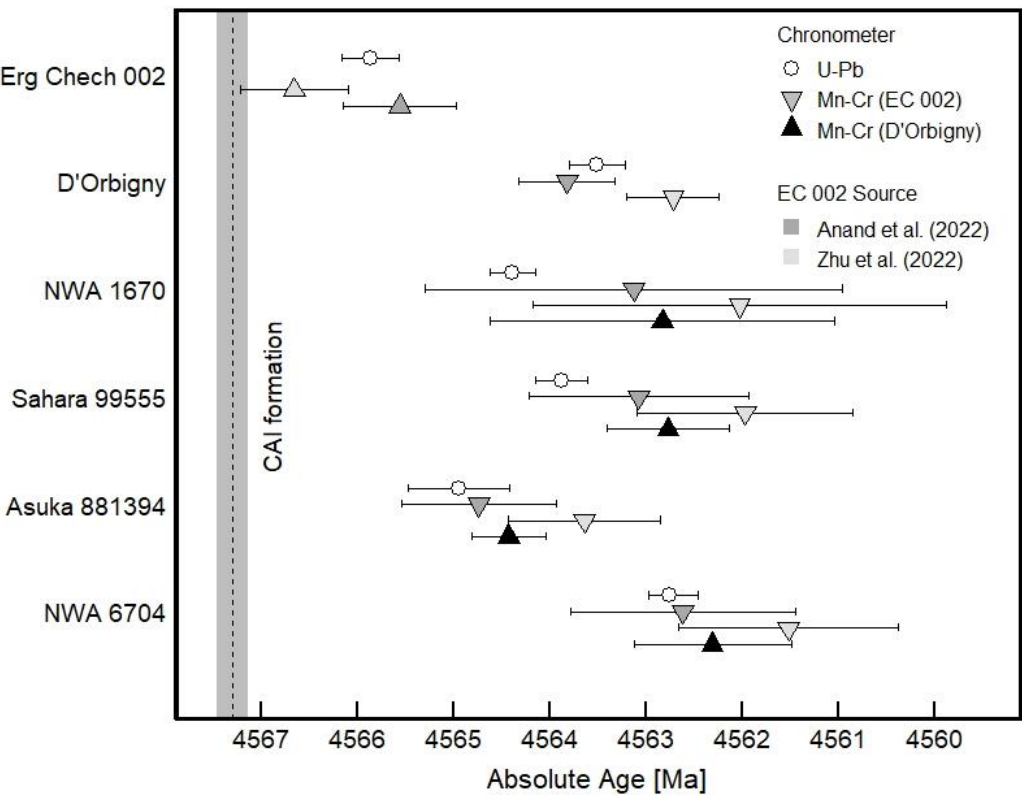


Figure 8: Age comparison between U-corrected Pb-Pb ages and ^{26}Al - ^{26}Mg ages anchored to EC 002 (4565.87 ± 0.30 Ma: this study), D'Orbigny (4563.51 ± 0.29 Ma: Amelin, 2008a; Tissot et al., 2017) and CAIs (4567.30 ± 0.30 : Connelly et al., 2012) of various achondrites. Data and their sources are presented in Table S3. For clarity, the plotted U-corrected Pb-Pb age of Sahara 99555 is the weighted mean of Amelin (2008a) and Connelly et al. (2008), corrected by Tissot et al. (2017). For Asuka 881394 and NWA 2976, the ^{26}Al - ^{26}Mg ages plotted are those reported by the same studies that reported their U-corrected Pb-Pb ages (Bouvier et al., 2011b; Wimpenny et al., 2019).

823

824



825

826

827

828

829

830

831

832

Figure 9: Age comparison between U-corrected Pb-Pb ages and ^{53}Mn - ^{53}Cr ages anchored to EC 002 (4565.87 ± 0.30 Ma: this study) and D'Orbigny (4563.51 ± 0.29 Ma: Amelin, 2008a; Tissot et al., 2017) of different achondrites, highlighting the ^{53}Mn - ^{53}Cr age differences between of Anand et al. (2022) (dark grey colouring) and Zhu et al. (2022) (light grey colouring). Data and their sources are presented in Table S3. For clarity, the U-corrected Pb-Pb age of Sahara 99555 plotted is the weighted mean of Amelin (2008a) and Connelly et al. (2008), corrected by Tissot et al. (2017).

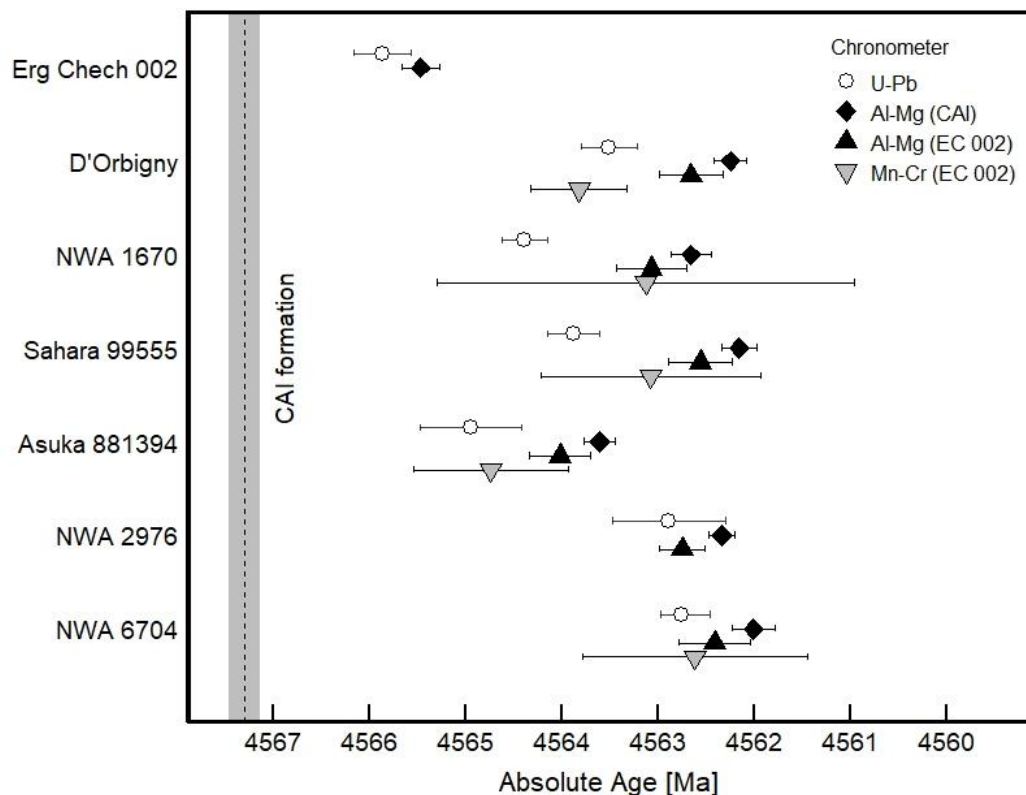


Figure 10: Age comparison between U-corrected Pb-Pb ages, and ^{26}Al - ^{26}Mg ages anchored to CAIs (4567.30 ± 0.30 : Connelly et al., 2012), and both ^{26}Al - ^{26}Mg and ^{53}Mn - ^{53}Cr ages anchored to EC 002 (4565.87 ± 0.30 Ma: this study) of various achondrites. Data and their sources are presented in Table S3. The initial $^{53}\text{Mn}/^{55}\text{Mn}$ ratio reported by Anand et al. (2022) is used to calculate ^{53}Mn - ^{53}Cr ages in this diagram. For clarity, the U-corrected Pb-Pb age of Sahara 99555 plotted is the weighted mean of Amelin (2008a) and Connelly et al. (2008), corrected by Tissot et al. (2017), and for Asuka 881394 and NWA 2976, the ^{26}Al - ^{26}Mg ages plotted are those reported by the same studies that reported their U-corrected Pb-Pb ages (Bouvier et al., 2011b; Wimpenny et al., 2019).

5. Conclusions

The ungrouped achondrite Erg Chech 002 was dated by U-corrected Pb-Pb and ^{26}Al - ^{26}Mg chronology in mineral and bulk rock fractions, as well as *in situ* U-Pb chronology of Ca-phosphates by SIMS. Compared to previous studies that dated EC 002 by *in situ* ^{26}Al - ^{26}Mg analysis (Barrat et al., 2021), the ^{26}Al - ^{26}Mg age was determined by MC-ICP-MS analysis of seven mineral fraction and results in an age that is 0.43 ± 0.11 Myr older, at 1.83 ± 0.12 Ma after CAI formation and an absolute age of 4565.47 ± 0.20 Ma when anchored to the absolute age of CAIs. This age is consistent with the reported ^{26}Al - ^{26}Mg age by Fang et al. (2022). The U-corrected Pb-Pb age of EC 002 is 4565.87 ± 0.30 Ma, determined by pyroxene residue and leachates, and makes EC 002 the oldest dated achondrite so far. The U isotope composition was determined for both a bulk rock and a leached pyroxene fraction, resulting in a notable difference between them that is likely caused by internal heterogeneities between mineral phases. For the calculation of the Pb-Pb age, the $^{238}\text{U}/^{235}\text{U}$ ratio of the (re-combined) leached pyroxenes was used.

The U-Pb age determined by *in situ* analysis of merrillites by SIMS is 4564.3 ± 5.2 Ma, equal within uncertainty to the U-corrected Pb-Pb age determined on leached pyroxenes. This indicates that the parent body of EC 002 was not exposed to thermal metamorphism or any substantial impact events after ~ 4559 Ma and underwent rapid cooling.

The good agreement between ^{26}Al - ^{26}Mg and U-corrected Pb-Pb ages of CC achondrites when anchored to EC 002, indicates that ^{26}Al was distributed homogeneously between the NC and CC reservoirs, in contrast to previous interpretations suggesting the opposite (e.g., Schiller et al., 2015). The age differences between ^{26}Al - ^{26}Mg and U-corrected Pb-Pb ages of angrites and NC achondrite Asuka 881394 when anchored to EC 002 and CAIs are most likely to have been caused by diffusion of Mg isotopes in plagioclase during re-heating episodes or later thermal events. The

concordance between ^{53}Mn - ^{53}Cr ages and U-corrected Pb-Pb ages of those same achondrites suggest that the ^{53}Mn - ^{53}Cr chronometer was not disturbed. Given its old age, precise ^{26}Al - ^{26}Mg and U-corrected Pb-Pb ages and straightforward thermal history, EC 002 shows promise to be used as an anchor to date other objects with short-lived chronometers.

Acknowledgements

We are thankful to Ben Hoefnagels (Big Bang meteorites) for the donation of a sample of Erg Chech 002. AB thanks support from the Canada Foundation for Innovation (Grant Agreement No. 33353), Government of Ontario (ER15-11-077), NSERC Discovery Grant (06310-2014) and Canada Research Chairs programs (950-229061), and Ning Ma, Detlef Krauß and Dorothea Wiesner for analytical support at BGI. PMR thanks the Ontario Graduate Scholarship program. MT and WHS thank support by Klaus Tschira Stiftung. We also thank three anonymous reviewers and associate editor Vinciane Debaille for providing constructive feedback and recommendations.

Appendix A. Supplementary Material

Table S1: EPMA elemental compositions of merrillites in EC 002.

Table S2: ^{26}Mg isotopic anomalies ($\delta^{26}\text{Mg}^*$) of EC 002 mineral fractions calculated with different fractionation (kinetic vs. equilibrium) factors.

Table S3: compilation of published U-corrected Pb-Pb ages, ^{26}Al - ^{26}Mg ages and ^{53}Mn - ^{53}Cr ages of EC 002 and other achondrites.

Figures S1 and S2: linearized three-isotope plots of Mg of individual analyses of rock standards San Carlos olivine and CV3 chondrite Allende, respectively.

References

- Abouchami W., Galer S. J. G. and Hofmann A. W. (2000) High precision lead isotope systematics of lavas from the Hawaiian Scientific Drilling Project. *Chem. Geol.* **169**, 187–209.
- Amelin Y. (2008a) The U-Pb systematics of angrite Sahara 99555. *Geochim. Cosmochim. Acta* **72**, 4874–4885.
- Amelin Y. (2008b) U-Pb ages of angrites. *Geochim. Cosmochim. Acta* **72**, 221–232.
- Amelin Y., Kaltenbach A., Iizuka T., Stirling C. H., Ireland T. R., Petaev M. and Jacobsen S. B. (2010) U-Pb chronology of the Solar System's oldest solids with variable $^{238}\text{U}/^{235}\text{U}$. *Earth Planet. Sci. Lett.* **300**, 343–350.
- Amelin Y., Koefoed P., Iizuka T., Fernandes V. A., Huyskens M. H., Yin Q. and Irving A. J. (2019) U-Pb, Rb-Sr and Ar-Ar systematics of the ungrouped achondrites Northwest Africa 6704 and Northwest Africa 6693. *Geochim. Cosmochim. Acta* **245**, 628–642.
- An Y. and Huang F. (2014) A review of Mg isotope analytical methods by MC-ICP-MS. *J. Earth Sci.* **25**, 822–840.
- Anand A., Kruttasch P. M. and Mezger K. (2022) ^{53}Mn - ^{53}Cr chronology and $\epsilon^{54}\text{Cr}$ - $\Delta^{17}\text{O}$ genealogy of Erg Chech 002: the oldest andesite in the Solar System. *Meteorit Planet Sci.*
- Ancellin M. A., Vlastélic I., Samaniego P., Nauret F., Gannoun A. and Hidalgo S. (2019) Up to 1% Pb isotope disequilibrium between minerals hosted in dacites from the Guagua Pichincha volcano, Ecuador: Implication for tracing the source and crustal history of continental arc magmas. *Chem. Geol.* **525**, 177–189.
- Barrat J., Chaussidon M., Yamaguchi A., Beck P., Villeneuve J., Byrne D. J., Broadley M. W. and Marty B. (2021) A 4,565-My-old andesite from an extinct chondritic protoplanet. *Proc. Natl. Acad. Sci.* **118**, e2026129118.

913 Blichert-Toft J., Zanda B., Ebel D. S. and Albarède F. (2010) The Solar System primordial lead.
 914 *Earth Planet. Sci. Lett.* **300**, 152–163.

915 Bollard J., Connelly J. N., Whitehouse M. J., Pringle E. A., Bonal L., Jørgensen J. K., Nordlund
 916 Å., Moynier F. and Bizzarro M. (2017) Early formation of planetary building blocks inferred
 917 from Pb isotopic ages of chondrules. *Sci. Adv.* **3**.

918 Bollard J., Kawasaki N., Sakamoto N., Olsen M., Itoh S., Larsen K., Wielandt D., Schiller M.,
 919 Connelly J. N., Yurimoto H. and Bizzarro M. (2019) Combined U-corrected Pb-Pb dating
 920 and ^{26}Al - ^{26}Mg systematics of individual chondrules – Evidence for a reduced initial
 921 abundance of ^{26}Al amongst inner Solar System chondrules. *Geochim. Cosmochim. Acta* **260**,
 922 62–83.

923 Bouvier A., Blichert-Toft J., Moynier F., Vervoort J. D. and Albarède F. (2007) Pb-Pb dating
 924 constraints on the accretion and cooling history of chondrites. *Geochim. Cosmochim. Acta*
 925 **71**, 1583–1604.

926 Bouvier A., Blichert-Toft J., Vervoort J. D. and Albarède F. (2005) The age of SNC meteorites
 927 and the antiquity of the Martian surface. *Earth Planet. Sci. Lett.* **240**, 221–233.

928 Bouvier A., Brennecka G. A. and Wadhwa M. (2011a) Absolute chronology of the first solids in
 929 the Solar System. In *Formation of the First Solids in the Solar System* p. 9054.

930 Bouvier A., Spivak-Birndorf L. J., Brennecka G. A. and Wadhwa M. (2011b) New constraints on
 931 early Solar System chronology from Al-Mg and U-Pb isotope systematics in the unique
 932 basaltic achondrite Northwest Africa 2976. *Geochim. Cosmochim. Acta* **75**, 5310–5323.

933 Bouvier A. and Wadhwa M. (2010) The age of the Solar System redefined by the oldest Pb – Pb
 934 age of a meteoritic inclusion. *Nat. Geosci.* **3**, 637–641.

935 Bouvier A., Wadhwa M., Simon S. B. and Grossman L. (2013) Magnesium isotopic fractionation

936 in chondrules from the Murchison and Murray CM2 carbonaceous chondrites. *Meteorit.*
 937 *Planet. Sci.* **48**, 339–353.

938 Brennecka G. A. and Wadhwa M. (2012) Uranium isotope compositions of the basaltic angrite
 939 meteorites and the chronological implications for the early Solar System. *Proc. Natl. Acad.*
 940 *Sci. U. S. A.* **109**, 9299–9303.

941 Brennecka G. A., Weyer S., Wadhwa M., Janney P. E., Zipfel J. and Anbar A. D. (2010) $^{238}\text{U}/^{235}\text{U}$
 942 variations in meteorites: Extant ^{247}Cm and implications for Pb-Pb Dating. *Science* (80-.).
 943 **327**, 449–451.

944 Catanzaro E. J., Murphy T. J., Garner E. L. and Shields W. R. (1966) Absolute Isotopic Abundance
 945 Ratios and Atomic Weight of Magnesium. *J. Res. Natl. Bur. Stand. Sect. A, Phys. Chem.* **70A**,
 946 453–458.

947 Catanzaro E. J., Murphy T. J., Shields W. R. and Garner E. L. (1968) Absolute isotopic abundance
 948 ratios of common, equal-atom, and radiogenic lead isotopic standards. *J. Res. Natl. Bur.*
 949 *Stand. - A Phys. Chem.* **72A**, 261.

950 Cherniak D. J. (2001) Pb diffusion in Cr diopside, augite, and enstatite, and consideration of the
 951 dependence of cation diffusion in pyroxene on oxygen fugacity. *Chem. Geol.* **177**, 381–397.

952 Connelly J. N. and Bizzarro M. (2009) Pb-Pb dating of chondrules from CV chondrites by
 953 progressive dissolution. *Chem. Geol.* **259**, 143–151.

954 Connelly J. N., Bizzarro M., Krot A. N., Nordlund Å., Wielandt D. and Ivanova M. A. (2012) The
 955 absolute chronology and thermal processing of solids in the solar protoplanetary disk. *Science*
 956 **338**, 651–655.

957 Connelly J. N., Bizzarro M., Thrane K. and Baker J. A. (2008) The Pb-Pb age of Angrite
 958 SAH99555 revisited. *Geochim. Cosmochim. Acta* **72**, 4813–4824.

959 Connelly J. N., Bollard J. and Bizzarro M. (2017) Pb–Pb chronometry and the early Solar System.
 960 *Geochim. Cosmochim. Acta* **201**, 345–363.

961 Connelly J. N., Schiller M. and Bizzarro M. (2019) Pb isotope evidence for rapid accretion and
 962 differentiation of planetary embryos. *Earth Planet. Sci. Lett.* **525**, 115722.

963 Fang L., Frossard P., Boyet M., Bouvier A., Barrat J.-A., Chaussidon M. and Moynier F. (2022)
 964 Half-life and initial Solar System abundance of ^{146}Sm determined from the oldest andesitic
 965 meteorite. *Proc. Natl. Acad. Sci.* **119**.

966 Floss C., Crozaz G., McKay G., Mikouchi T. and Killgore M. (2003) Petrogenesis of angrites.
 967 *Geochim. Cosmochim. Acta* **67**, 4775–4789.

968 Gattacceca J., McCubbin F. M., Grossman J., Bouvier A., Bullock E., Chennaoui Aoudjehane H.,
 969 Debaille V., D’Orazio M., Komatsu M., Miao B. and Schrader D. L. (2021) The Meteoritical
 970 Bulletin, No. 109. *Meteorit. Planet. Sci.* **56**, 1626–1630.

971 Glavin D. P., Kubny A., Jagoutz E. and Lugmair G. W. (2004) Mn–Cr isotope systematics of the
 972 D’Orbigny angrite. *Meteorit. Planet. Sci.* **39**, 693–700.

973 Gregory T., Luu T.-H., Coath C. D., Russell S. S. and Elliott T. (2020) Primordial formation of
 974 major silicates in a protoplanetary disc with homogeneous $^{26}\text{Al}/^{27}\text{Al}$. *Sci. Adv.* **6**, eaay9626.

975 Hublet G., Debaille V., Wimpenny J. and Yin Q. Z. (2017) Differentiation and magmatic activity
 976 in Vesta evidenced by ^{26}Al – ^{26}Mg dating in eucrites and diogenites. *Geochim. Cosmochim.*
 977 *Acta* **218**, 73–97.

978 Huyskens M. H., Amelin Y. and Yin Q.-Z. (2020) Uranium Isotopic Composition of Angrites. In
 979 *Lunar and Planetary Science Conference* p. 1781.

980 Ito K., Hibiya Y., Homma Y., Mikouchi T. and Iizuka T. (2019) The promise and potential pitfalls
 981 of acid leaching for Pb–Pb chronology. *Chem. Geol.* **525**, 343–355.

982 Jacobsen B., Yin Q. zhu, Moynier F., Amelin Y., Krot A. N., Nagashima K., Hutcheon I. D. and
 983 Palme H. (2008) ^{26}Al - ^{26}Mg and ^{207}Pb - ^{206}Pb systematics of Allende CAIs: Canonical solar
 984 initial $^{26}\text{Al}/^{27}\text{Al}$ ratio reinstated. *Earth Planet. Sci. Lett.* **272**, 353–364.

985 Kawasaki N., Park C., Sakamoto N., Young S., Na H., Kuroda M. and Yurimoto H. (2019)
 986 Variations in initial $^{26}\text{Al}/^{27}\text{Al}$ ratios among fluffy Type A Ca–Al-rich inclusions from reduced
 987 CV chondrites. *Earth Planet. Sci. Lett.* **511**, 25–35.

988 Kawasaki N., Wada S., Park C., Sakamoto N. and Yurimoto H. (2020) Variations in initial
 989 $^{26}\text{Al}/^{27}\text{Al}$ ratios among fine-grained Ca-Al-rich inclusions from reduced CV chondrites.
 990 *Geochim. Cosmochim. Acta* **279**, 1–15.

991 Keil K. (2012) Angrites, a small but diverse suite of ancient, silica-undersaturated volcanic-
 992 plutonic mafic meteorites, and the history of their parent asteroid. *Chemie der Erde* **72**, 191–
 993 218.

994 Kita N. T., Yin Q. Z., Macpherson G. J., Ushikubo T., Jacobsen B., Nagashima K., Kurahashi E.,
 995 Krot A. N. and Jacobsen S. B. (2013) ^{26}Al - ^{26}Mg isotope systematics of the first solids in the
 996 early solar system. *Meteorit. Planet. Sci.* **48**, 1383–1400.

997 Koefoed P., Amelin Y., Yin Q. Z., Wimpenny J., Sanborn M. E., Iizuka T. and Irving A. J. (2016)
 998 U-Pb and Al-Mg systematics of the ungrouped achondrite Northwest Africa 7325. *Geochim.*
 999 *Cosmochim. Acta* **183**, 31–45.

1000 Krot A. N., Petaev M. I. and Nagashima K. (2021) Infiltration metasomatism of the Allende
 1001 coarse-grained calcium-aluminum-rich inclusions. *Prog. Earth Planet. Sci.* **8**, 61.

1002 Kruijer T. S., Kleine T. and Borg L. E. (2020) The great isotopic dichotomy of the early Solar
 1003 System. *Nat. Astron.* **4**, 32–40.

1004 Larsen K. K., Trinquier A., Paton C., Schiller M., Wielandt D., Ivanova M. A., Connelly J. N.,

1005 Nordlund Å., Krot A. N. and Bizzarro M. (2011) Evidence for Magnesium Isotope
 1006 Heterogeneity in the Solar Protoplanetary Disk. *Astrophys. J.* **735**, L37.
 1007 Ludwig K. R. (2008) Isoplot version 4.15: a geochronological toolkit for microsoft Excel. *Berkeley*
 1008 *Geochronol. Center, Spec. Publ.*, 247–270.
 1009 MacPherson G. J., Bullock E. S., Tenner T. J., Nakashima D., Kita N. T., Ivanova M. A., Krot A.
 1010 N., Petaev M. I. and Jacobsen S. B. (2017) High precision Al–Mg systematics of forsterite-
 1011 bearing Type B CAIs from CV3 chondrites. *Geochim. Cosmochim. Acta* **201**, 65–82.
 1012 Marsh S. F., Alarid J. E., Hammond C. F., McLeod M. J., Roensch F. R. and Rein J. E. (1978)
 1013 *Anion exchange of 58 elements in hydrobromic acid and in hydriodic acid.*, Los Alamos, NM.
 1014 Merle R., Amelin Y., Yin Q.-Z., Huyskens M. H., Sanborn M. E., Nagashima K., Yamashita K.,
 1015 Ireland T. R., Krot A. N. and Sieber M. J. (2020) Exploring the efficiency of stepwise
 1016 dissolution in removal of stubborn non-radiogenic Pb in chondrule U-Pb dating. *Geochim.*
 1017 *Cosmochim. Acta* **277**, 1–20.
 1018 Nicklas R. W., Day J. M. D., Gardner-Vandy K. G. and Udry A. (2022) Early silicic magmatism
 1019 on a differentiated asteroid. *Nat. Geosci.*, *15*(9), 696-699.
 1020 Nyquist L. E., Reese Y., Wiesmann H., Shih C. Y. and Takeda H. (2003) Fossil ²⁶Al and ⁵³Mn in
 1021 the Asuka 881394 eucrite: Evidence of the earliest crust on asteroid 4 Vesta. *Earth Planet.*
 1022 *Sci. Lett.* **214**, 11–25.
 1023 Richter S., Eykens R., Kühn H., Aregbe Y., Verbruggen A. and Weyer S. (2010) New average
 1024 values for the n(²³⁸U)/n(²³⁵U) isotope ratios of natural uranium standards. *Int. J. Mass*
 1025 *Spectrom.* **295**, 94–97.
 1026 Roebbert Y., Rosendahl C. D., Brown A., Schippers A., Bernier-Latmani R. and Weyer S. (2021)
 1027 Uranium isotope fractionation during the anoxic mobilization of noncrystalline U(IV) by

1028 ligand complexation. *Environ. Sci. Technol.* **55**, 7959–7969.

1029 Sanborn M. E., Carlson R. W. and Wadhwa M. (2015) ^{147}Sm – ^{143}Nd , ^{176}Lu – ^{176}Hf , and ^{87}Rb –
1030 ^{87}Sr systematics in the angrites: Implications for chronology and processes on the angrite
1031 parent body. *Geochim. Cosmochim. Acta* **171**, 80–99.

1032 Sanborn M. E., Wimpenny J., Williams C. D., Yamakawa A., Amelin Y., Irving A. J. and Yin Q.
1033 (2019) Carbonaceous achondrites Northwest Africa 6704/6693: Milestones for early Solar
1034 System chronology and genealogy. *Geochim. Cosmochim. Acta* **245**, 577–596.

1035 Schiller M., Baker J. A. and Bizzarro M. (2010a) ^{26}Al – ^{26}Mg dating of asteroidal magmatism in the
1036 young Solar System. *Geochim. Cosmochim. Acta* **74**, 4844–4864.

1037 Schiller M., Bizzarro M. and Fernandes V. A. (2018) Isotopic evolution of the protoplanetary disk
1038 and the building blocks of Earth and the Moon. *Nature* **555**, 507–510.

1039 Schiller M., Connelly J. N., Glad A. C., Mikouchi T. and Bizzarro M. (2015) Early accretion of
1040 protoplanets inferred from a reduced inner solar system ^{26}Al inventory. *Earth Planet. Sci.*
1041 *Lett.* **420**, 45–54.

1042 Schiller M., Handler M. R. and Baker J. A. (2010b) High-precision Mg isotopic systematics of
1043 bulk chondrites. *Earth Planet. Sci. Lett.* **297**, 165–173. Available at:
1044 <http://dx.doi.org/10.1016/j.epsl.2010.06.017>.

1045 Sedaghatpour F. and Teng F. Z. (2016) Magnesium isotopic composition of achondrites. *Geochim.*
1046 *Cosmochim. Acta* **174**, 167–179.

1047 Spivak-Birndorf L., Wadhwa M. and Janney P. (2009) ^{26}Al – ^{26}Mg systematics in D’Orbigny and
1048 Sahara 99555 angrites: Implications for high-resolution chronology using extinct
1049 chronometers. *Geochim. Cosmochim. Acta* **73**, 5202–5211.

1050 Stacey J. S. and Kramers J. D. (1975) Approximation of terrestrial lead isotope evolution by a two-

stage model. *Earth Planet. Sci. Lett.* **26**, 207–221.

Steiger R. H. and Jäger E. (1977) Subcommittee on geochronology: convention on the use of decay constants in geo- and cosmochemistry. *Earth Planet. Sci. Lett.* **36**, 359–362.

Stirling C. H., Halliday A. N. and Porcelli D. (2005) In search of live ^{247}Cm in the early solar system. *Geochim. Cosmochim. Acta* **69**, 1059–1071.

Sugiura N., Miyazaki A. and Yanai K. (2005) Widespread magmatic activities on the angrite parent body at 4562 Ma ago. *Earth, Planets Sp.* **57**, 13–16.

Tatsumoto M., Knight R. J. and Allegre C. J. (1973) Time Differences in the Formation of Meteorites as Determined from the Ratio of Lead-207 to Lead-206. *Science* (80-.). **180**, 1279–1283.

Teng F.-Z., Wadhwa M. and Helz R. T. (2007) Investigation of magnesium isotope fractionation during basalt differentiation: Implications for a chondritic composition of the terrestrial mantle. *Earth Planet. Sci. Lett.* **261**, 84–92.

Teng F. Z., Li W. Y., Ke S., Marty B., Dauphas N., Huang S., Wu F. Y. and Pourmand A. (2010) Magnesium isotopic composition of the Earth and chondrites. *Geochim. Cosmochim. Acta* **74**, 4150–4166.

Thomson S. N., Gehrels G. E., Ruiz J. and Buchwaldt R. (2012) Routine low-damage apatite U-Pb dating using laser ablation-multicollector- ICPMS. *Geochemistry, Geophys. Geosystems* **13**, 1–23.

Tissot F. L. H., Dauphas N. and Grossman L. (2016) Origin of uranium isotope variations in early solar nebula condensates. *Sci. Adv.* **2**, 1–8.

Tissot F. L. H., Dauphas N. and Grove T. L. (2017) Distinct $^{238}\text{U}/^{235}\text{U}$ ratios and REE patterns in plutonic and volcanic angrites: Geochronologic implications and evidence for U isotope